Technische Universität München
Photogrammetry and Remote Sensing
Prof. Dr.-Ing. U. Stilla

Change Detection of Buildings using Satellite Images and DSMs

Divyesh Varade

Master Thesis

Start - End: 24.05. 2011 – 24. 10. 2011

Program: ESPACE - Earth oriented space science and technology (Master)

Supervisor(s): Prof. Dr.-Ing. Uwe Stilla (TUM) ,
Msc.-Ing Jiaojiao Tian (DLR)
Dipl.-Ing Michael Schmitt (TUM),

Cooperation: DLR Institut für Methodik der Fernerkundung

2011

ABSTRACT

Change Detection techniques play a very significant role in modern infrastructure especially in urban areas. Urban areas are often reconstructed to replenish with greater space and resources. In urban areas most common and significant objects of interest are buildings. With advancements in remote sensing technologies, change detection based on high resolution satellite images provides an efficient tool for monitoring infrastructural development within vast premises. Since visual analysis is costly and impractical, several automatic and semi automatic methods have been researched for change detection. Although there are a number of such methods, their applicability is restrained by limitation of the data they are evaluated upon. For example in case of buildings often real changes are mixed with other land cover changes, especially manmade structures such as roads, bridges etc due to their resemblance in the captured images. Although it is possible to eliminate these errors with height information from DSMs, the accuracy is directly proportional to the quality of the DSMs. Hence it also becomes crucial to develop highly sophisticated change detection methods based alone on the images.

This study corresponds to another semi-automatic method that uses information similarity measures for change detection. Information similarity measures are commonly used individually for image segmentation and often for change detection. The approach followed here combines several information similarity measures to enhance a basic change map developed from simple differencing simultaneously incorporating height information from DSMs to assess changes in both horizontal as well as vertical direction. Firstly an initial estimate of the building changes is generated using simple differencing of the DSMs, followed by elimination of shadows and vegetation that may cause misinterpretation as changed buildings otherwise. The pixels from the initial estimate are then used as seed in a sliding window algorithm for supplementary change detection with information similarity measures using the gray early and late images. The different information similarity measures are combined to estimate a tradeoff parameter which is used for developing the change map. With increase in the availability of DSMs generated from automatic techniques using optical stereo high resolution satellite imagery, such processing becomes more feasible.

In this study the developed approach is successfully tested on two data sets from Eastern Asia and Munich, Germany. The efficiency of different information similarity measures were tested by experimenting with training areas selected from the processed DSM difference. Pixels that are changed and those which are unchanged are analyzed together. The effectiveness of the presented approach was evaluated through pixel based assessment, as well as object based assessment. The different information similarity measures i.e. Kullback Leibler Divergence, Jenson Shannon Divergence, Chi-square Divergence and Cluster Reward Algorithm were also assessed individually for each data set. Also the influence of DSMs within the process of change detection was analyzed and s significant.

Keywords: Building Change detection, DSMs, VHR, image differencing, Mutual Information, Kullback Leibler Divergence, Cluster Reward Algorithm, Jenson Shannon Divergence.

DECLARATION

This thesis is a presentation of my original research work. Wherever contributions of others are involved, every effort is made to indicate this clearly, with due reference to the literature, and acknowledgement of collaborative research and discussions.

Munich October 2011

Divyesh Varade

ACKNOWLEDGEMENTS

I would like to hereby express my gratitude to all the people involved in the help of my thesis.

First of all, I would like to express my sincere thanks to Prof. Dr. Uwe Stilla for supervising this study, Msc.-Ing Jiaojiao Tian and Prof. Dr.-Ing Peter Reinartz for giving me an opportunity to undertake this thesis at the Photogrammetry and Image Analysis Dept. in DLR and for providing invaluable and suggestions during this research. I would like to thank Thomas Krauß and Pablo d'Angelo for providing me with the necessary test data and DSMs respectively for this study. I would also like to thank Dipl. -Ing. Michael Schmitt for his patient supervision during this thesis. I have obtained immense support during this thesis including the valuable guidance and advices that have helped in various deadlocks during this study.

Furthermore I would like to thank Shiyong Cui for his constructive recommendations during the period of this work. Also I would here by like to thank Dr. Danielle Hoja for her valuable assistance and moral support.

Last but not least, I want to thank my parents, my colleagues and my friends for their love and support during my studies in Germany. Whenever I faced a stranglehold, they have always given me immense support and encouragement in my life.

TABLE OF CONTENTS

LIST OF FIGURES

LIST OF TABLES

1. INTRODUCTION

1.1 Motivation

With current scenarios urban areas often undergo reconstruction to implement proficient spatial and resource management. The major emphasis in analyzing urban areas is usually on buildings and roads which characterize the infrastructural aspects for an area. The analysis of buildings is also significant for city modeling, urban planning and damage analysis. For urban planning it thus becomes extremely crucial to identify the changes occurring during the recuperation phase. Change detection methods play a significant part in such analysis. These techniques provide the measures to supervise and monitor areas under reconstruction. This includes development of buildings roads etc. Change detection methods are also used with a variety of objects under consideration, such as in monitoring the extent of forestation and de-forestation in forestry or monitoring the infrastructural development by extracting demolished and reconstructed buildings, roads etc.

Change detection procedures usually analyze a specific topographical aspect of an area, which in case of urban areas are most commonly the buildings. Most techniques use analytic methods on multi-date images for change detection which characterizes the nature of change in horizontal directions i.e. in two dimensions (2D). Some of these methods were compared in a review by Coppin et al. (2004). Mutual Information and divergence measures such as the Kullback Leibler Divergence are often used for image matching (Kim et al. 2003; Hirschmüller 2008; Goldberger et al. 2003) and can also be used on a pixel by pixel basis for change detection as illustrated by Cui et al. (2011) in a probabilistic way (Bruzzone & Prieto 2000).

Although 2D change detection methods are sufficiently efficient they may often be flawed. In 2D change detection of buildings, often apparently gray building roofs or terrace vegetation are confused with other objects such as roads or gardens. Thus accurate identification of actual changes requires additional information than just multi-date images. 2D change detection methods can be combined with additional information to provide further details on building changes along with increasing the accuracy of detection. Lin et al. (2009) use 3D data along with 2D image analysis to classify various changes in buildings. Tian et al. (2010) and Chaabouni-Chouayakh et al. (2011) use Digital Surface Models (DSMs) for such analysis. Thus by incorporating additional height information from DSMs into change detection not only the accuracy can be substantially increased, but also changes are observed in both horizontal (2D) as well as vertical (3D) direction. Hence DSMs hold immensely significant influence regarding change detection. Such implementation of DSMs for change detection is especially more feasible with the advances in DSM generation techniques (Hirschmüller 2008; Krauß et al. 2007; d' Angelo 2010) and the increasingly available DSMs generated from space borne optical stereo images from satellites such as IKONOS and WORLDVIEW-2. In comparison to LIDAR such DSMs are also highly cost efficient. Although the quality of such DSMs is lower compared to LIDAR DSMs, this can be compensated with improvement in the 2D change detection method employed.

The proposed approach here focuses on extraction of changes in buildings in urban areas. A 2D change map can be generated using information theoretical measures (Bruzzone & Prieto 2000; Kim et al. 2003). A further task is to combine information from low quality DSMs generated from optical stereo satellite imagery, with such a change map to derive accurate changes in buildings in urban areas. Thereby analysis is carried out to accomplish a minimum possible count for false alarms and missed alarms and higher accuracy in detection of changes in buildings. The intermediate results shall be visualized on a change-map, and the changed buildings shall be classified into various change classes. Final results shall be based on pixel wise and object wise evaluation of the change-map with respect to the reference data. Also a comparison between the results from the various information similarity measures involved in this thesis is included. An assessment analysis shall be carried out based upon statistical and classification accuracy.

1.2 State of the Art

Comprehensive studies and research has been carried out associated to change detection in various sets of areas. Since the area of application for change detection varies from multi-image analysis to videos, there are many applied algorithms selectively suitable for a particular case. Since the generation of multi-temporal reference data is usually a complicated task along with the fact that it is expensive, the unsupervised change detection methods are thus commonly applicable and preferable in most cases. The simplest methods include differencing or ratioing of two images taken at different times followed by thresholding. Since the obtained results are very crude for any significant target identification, such a method is only a pre-detection step in various algorithms. Bruzzone & Prieto (2000) shows two methods of enhancing the change map developed from simple differencing (SD) by using probability estimation based on the difference image and the other using contextual information locally. Hence the general idea of enhancing a change detection map obtained from simple differencing is appropriately conceived.

Since change detection is a very common approach followed in various fields of research many methods have been developed. Singh (1989) described the initial techniques for change detection, such as Vegetation Index Differencing (VID), Principal Component Analysis (PCA), and Post-classification Comparison (PCC) etc. Mas (1999) provide a comparison between some of the methods illustrated by Singh (1989). A similar comparison of such methods was carried out by Coppin et al. (2004) and Lu et al. (2005). The generalized expression was to affirm that simpler methods such as SD or VID have insignificant results as compared to other methods such as PCA. Besides, other methods were also introduced based on information and statistical theory. Mostly the idea is to use similarity based measures for change detection such that similar pixels have a relatively fixed metric value based on these similarity measures dependent upon the individual gray value of the pixels. Statistical parameters such as mutual information are used for matching images for image registration. These parameters can also be used for change detection. These include the information similarity measures such as mutual information (Jahari et al. 2008), Kullback Leibler Divergence (Mercier et al. 2008) etc. and distance measures such as Chi-square (Inglada & Giros 2004), Bhattacharya Distance (Benedek et al. 2009), and CRA-Cluster Reward Algorithm (Alberga 2009) etc. The fore-mentioned measures can be classified based on the structure of their model, for example CRA and mutual

information both incorporate the joint probability along with marginal probability while others utilize only marginal probabilities.

Similarity measures in information theory are able to illustrate the amount of variation or similarity between the probability distributions for two images for change detection. Mutual information is often used by many researchers for such a purpose. Although mutual information is one of the most efficient methods for image registration as delineated by Suri & Reinartz (2010), it is also a measure used significantly for change detection (Jahri et al. 2008). Lafaix & Bosser (2009) use mutual information between two SAR images to characterize the changes in a given landscape. In literature usually mutual information is mostly used with SAR data. However, Cui et al. (2011) illustrate that the developments from mutual information are well applicable on optical images. Similarly other functions such as the Kullback Leibler Divergence are also employed in change detection applications. Inglada (2009) depicts such an application on multi-date SAR image. Gueguen et al. (2010) define the concept of mixed information derived from mutual information and joint entropy between two images for change detection and compares it with Kullback Leibler Divergence. Another such measure that utilizes the joint probability density to signify the similarity between two images is the Cluster Reward Algorithm (Alberga 2009; Inglada & Giros 2004). The cluster reward algorithm defines an index to distinguish between similar and different regions in an image. Inglada & Giros (2004) use different similarity measures for image registration. Although different measures are suitable for change detection, the object of interest may vary with each. However it would be appropriate to state that the type and quality of the data and the targeted object largely determine the suitability of a method and hence the same approach can be well recognized for change detection of buildings in urban areas.

In order to estimate the mentioned similarity measures the initial step is to estimate the marginal and joint probability density for the images under experiment. Bruzzone & Prieto (2000) utilize the expectation maximization algorithm to enhance the initial estimate of the probability density using histogram thresholding. Suri & Reinartz (2010) suggest using the histogram for estimating the probability distribution as one of the simple approaches. Rajwade et al. (2009) proposes an approach to determine the marginal and joint probability based on iso-contours and iso-surfaces.

When the observed objects consist of regions of appreciable size, a neighborhood processing algorithm is well suited. Okhandiar et al. (2006) use neighborhood correlation analysis for change detection. Cui et al. (2011) also use local information measures, specifically mutual information and the Kullback Leibler Divergence on multi-date optical stereo images and global approximation of mixed information by solving an over determined system of equations obtained from local measures.

Even though sufficient evidence is obtained in order to make a decision for apparent changes, usually several pixels on the change map are incorrectly classified for changes. For example if the same methods are used on two images, one taken in summer and the other taken in heavily snowed winter, than the areas without changes may be characterized by the 2D change detection algorithm as changes as was in our case. Hence it is appropriate to state that 2D

change detection algorithms classify changes in horizontal directions and evidently it becomes more significant to adopt measures to classify changes in vertical directions, i.e. with respect to target height and not only horizontal space occupied. This is possible by incorporation of DSMs.

With several DSM generation techniques (Hirschmüller 2008; Krauß et al. 2007; d'Angelo 2010) and the increasingly available DSMs generated from space borne optical stereo images from satellites such as IKONOS and WORLDVIEW-2 incorporation of DSMs for analysis. Some of these methods already use the information measures for stereo image matching (Suri & Reinartz 2010; Hirschmüller 2008). Thus they support the decision for selecting methods based on information theory change detection. However the resolution and the quality of the DSM is an issue to be considered. When the available DSMs are of low quality then methods with higher accuracy with respect to 2D change detection are required.

1.3 Problem Identification

High Resolution satellite data has greater clarity but is incorporated with several errors and noise. Such factors become critical for research areas such as change detection. While it is desired to reduce wrongly detected change pixels, there is a trade off to balance also the number of pixels that are missed in doing so. Usually most change detection algorithms target a particular object of interest such as buildings as in this study and in that case vegetation, cars etc becomes a major source of errors in detecting real changes. While the DSM difference provides a good idea regarding the changed regions, it often incorporates noise and error due to atmospheric conditions during image capture, mismatching etc. Thus supplementary change detection is often required besides the DSM difference to accurately classify changes.

1.4 Structure of the thesis

This research is illustrated in five chapters. Chapter 1 illustrates the motivation for this research, the state of the art and the problem statement associated to change detection. The theoretical background and the employed methodology are explained in Chapter 2. Chapter 3 delineates the data sets that are used to test and analyze the researched method. The experiments conducted for the classification of changes are elaborated in Chapter 4. The results obtained by implementation of the researched method are displayed and discussed in Chapter 5. At the end conclusions are derived and future possible work related to this research is discussed.

2. METHODOLOGY

The objective of change detection is to detect significant changes while rejecting insignificant ones within a observed area. In this work we are only concerned with building changes in urban areas from satellite imagery and the DSMs generated with stereo imagery. Usually change detection involves analysis of two matched and co-registered images of the observed geographical area taken at two different dates; we refer to them as early and late date images, if bi temporal images are considered. In this case the usual aim is to identify land cover changes (specifically buildings in this study) in study area between the two dates by using the reflected gray values in the optical images and combining information from DSMs. It is to be noted that before analysis on the images it is of immediate requirement to enhance the quality of the images in aimed areas. This is described in the following section under “Data Preprocessing”.

In literature, various approaches to change detection are classified mainly into supervised and unsupervised approaches (see figure 1). The former requires knowledge on the user’s part while the latter rather performs change detection by making a direct comparison of the two multispectral images considered, without relying on any additional information. Since the analysis of training areas for supervised classification is usually a complicated task along with the fact that it is expensive, the unsupervised change detection methods are usually commonly applicable and preferable in most cases. The major objective in these techniques is to identify the “change” pixels from “no change” pixels such that the pixel values of these two classes of pixels attain significantly different values.

Figure 1: Classification – Change Detection Techniques

The basic flow chart for such change detection techniques which involves information from both satellite images and DSMs is shown in figure 2. The early and late images are firstly preprocessed. In preprocessing the two images are ortho-rectified and co-registered followed by radiometric or intensity normalization (Radke 2005). The stereo images are used to generate the DSMs using the semi-global matching (Hirschmüller 2008) method. Afterwards the images and the corresponding DSMs can be used in the change detection algorithm for the development of a change map.

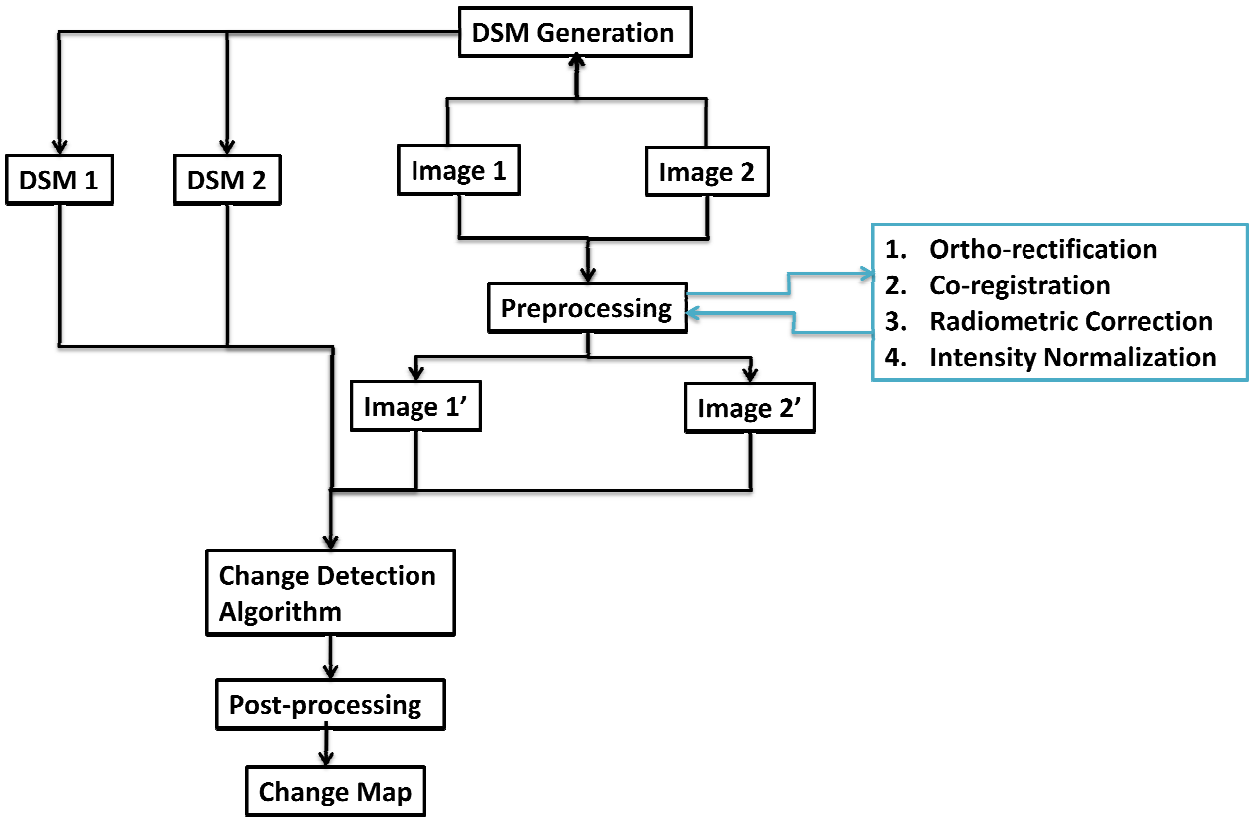

Figure 2: Basic Flow chart for change detection

2.1 Data Preprocessing

When using multi date imagery, ideally desired they must have similar characteristics based on intensity reflectance. However this is usually not true even for the images captured by the same sensor. Hence if it is desired to use such data for quantitative or qualitative analysis, the radiometric characteristics must be rendered similar by some compensational techniques. Mas (1999) explains two ways to achieve this radiometric compensation –

a) "Performing Radiometric Calibration, converting the entire dataset from digital number values into ground reflectance values.
b) Performing a relative radiometric normalization between the multi-date images."

However radiometric calibration is of significance for change detection especially when considering 2D techniques utilizing the gray values for example using the woods criterion (Alberga 2009). A suggested technique is the Automated Scattergram Controlled Regression developed by Elvidge et al. (1995). The same spectral band of two dates was used by J.F. Mas(1999) in order to produce a scattergram and define the regression line. He used the following step to define the regions of `no-change' using the scattergram. The pixels close to the regression line were assumed by him to be the ones without changes between the two dates and therefore used to perform the radiometric normalization. A histogram-matching procedure is another means to carry out the relative image-to-image radiometric normalization. Histograms of the digital numbers within the two multi-date images, master and slave, were computed.

Histograms were based on values from pixels belonging to the subarea that has been selected and labeled as `unchanged' on the scattergram analysis.

Besides radiometric correction accurate co-registration also proves to be significant. There should be sub-pixel level co-registration between the early and late images ideally. Since most change detection techniques are based on pixel by pixel analysis, correct co-registration is extremely important. Otherwise the two pixels compared in the change detection technique may not correspond to the same geographical region. In this case many false building changes may be observed or else many changes may be missed in the change detection.

2.2 Workflow

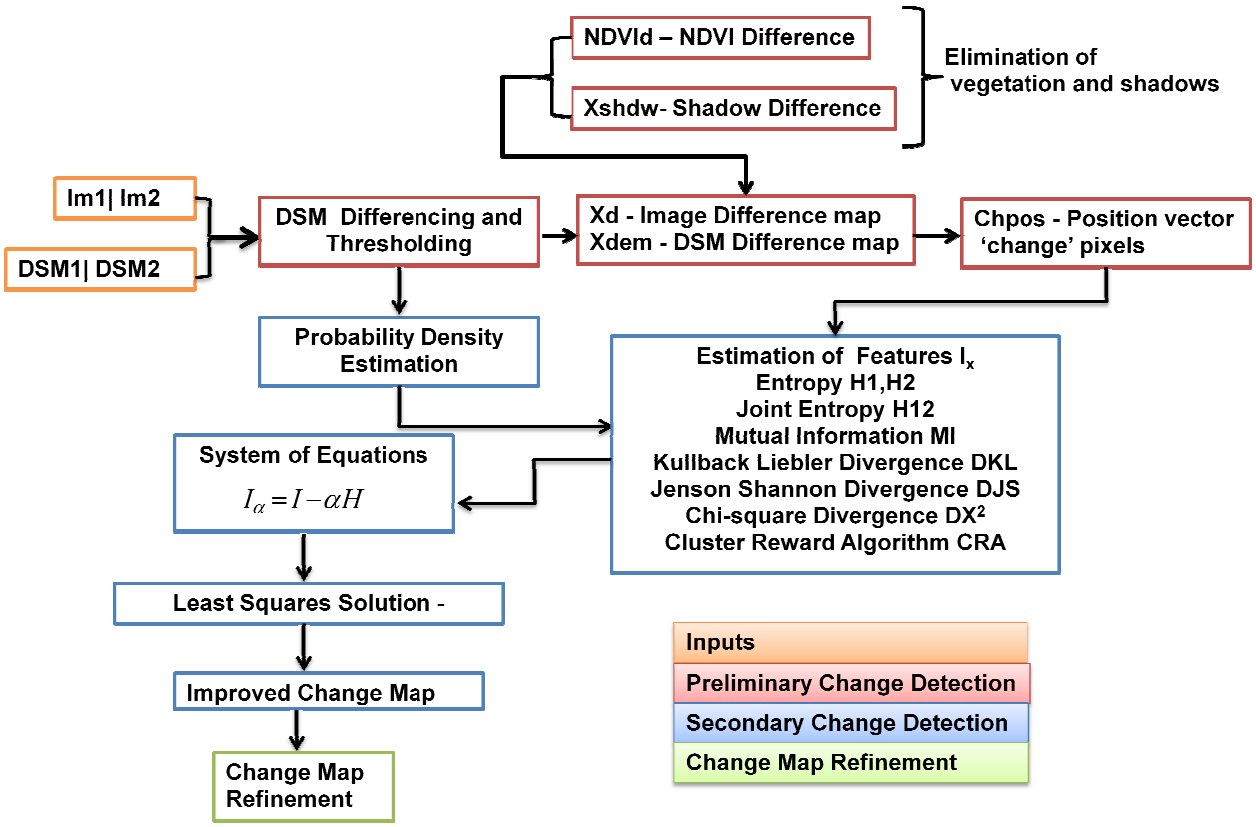

Figure 3: Workflow of the approach

The detailed workflow in figure 3 shows the approach used in this study for change detection. The initial step follows the preliminary building change detection. Within this stage the stereo images and the respective DSMs are differenced and thresholded based on the histogram. As a result an initial thresholded difference map is obtained, which provides the initial guess regarding pixels that may belong to the change map. This difference map provides the position vector that holds these possible change pixels. Since in this work the object of interest are buildings alone vegetation can well be eliminated. This is possible with the availability of multispectral images as in this case. It is explained in detail in section 3. Similarly the shadows may also affect the decision whether a pixel belongs to the change class or not. Since the

method is dependent upon the gray values of the pixel. Hence elimination of the shadows is also crucial.

The secondary building change detection process follows a sliding window algorithm, where the probability density for both images is estimated using the histogram for a predetermined neighborhood size. Once the probably estimates are obtained the various features involved in the method are estimated to obtain a system of equations, the solution to which determines the change map. The obtained change map is refined by eliminating minute regions if existent, since it can be assumed that they are unlikely any changed buildings.

2.3 Preliminary Change Detection

The preliminary building change detection refers to methods used for the initial approximation of the change mask. The result provides an initial guess of the pixels that may belong to change class. The stages within the preliminary change detection are explained in the following sections.

Generation of the Initial Change Map

A basic change detection algorithm generates a binary change mask as an output. Let $\{I_1, I_2\}$ be the set of early and late image maps a pixel coordinate $x \in R^l$ to intensity $I(x) \in R^k$ where *k* = *1*, for panchromatic images and *l* = *2* for 2D co-ordinate systems then the binary change mask $B(x)$ is defined as follows

$$B(x) = \begin{cases} 1 & Changed \\ 0 & Unchanged \end{cases}$$

..... **(1)**

The initial change map can be developed by simple techniques such as simple differencing of DSM explained in the next section. The resultant change map provides the positions of possible change pixels stored in a vector which is used for secondary change detection.

In a similar way the final change map can also be represented as follows

$$B(x) = \begin{cases} 1 \;\; PositiveChanges \\ 0 \;\; No \;\; Changes \\ -1 \;\; Negative \;\; Changes \end{cases}$$

..... **(2)**

In this case the change map represents a signum function where the ‘1’,’0’ and ‘-1’ represent the positive, unchanged and negatively changed regions. The positive changes may represent for example newly constructed buildings or reconstructed buildings, while the negative changes represent for example demolished buildings. Such a change mask provides not only the classification between the changed and unchanged regions but also categorizes the changes

into ‘positive changes’ and ‘negative changes’. This is especially productive when the data under investigation has both positive and negative changes for example in case of a demolished and reconstructed building.

2.3.1 Simple Differencing:

In this approach, the image taken at earlier date is subtracted pixel wise directly from the one taken at a later date (equation 3). Simple differencing is one of the simplest ways of generating a change mask. Similarly taking the ratio of the late and early image can also identify changes.

$$D_i(x) = I_2(x) - I_1(x) \quad \text{..... (3)}$$

$$D_{DSM}(x) = DSM_2(x) - DSM_1(x) \quad \text{..... (4)}$$

The same procedure is followed with the DSM, where the DSM difference shall provide the changes in vertical direction (equation 4).

2.3.2 Thresholding

The obtained change mask has potential changed pixels along with pixels that may not actually be real changed pixels. In order to eliminate these false change points post processing is required. Generally the change mask is thresholded to remove these unwanted pixels. The histogram of the DSM difference and the image difference is used to select the thresholds respectively for the DSM difference and image difference. A positive and negative threshold is selected manually for the positive and negative regions in the histogram or the difference image or DSM. Figure 4 shows an example of such an illustration. The initial threshold is determined by using Otsu’s method and then the threshold is increased or decreased while simultaneously the thresholded binary mask is checked visually until satisfactory (see Appendix A). Usually the values in bins closer to ‘0’ are often considered as unwanted in to the change classification. Hence thresholds are selected such that these values are eliminated.

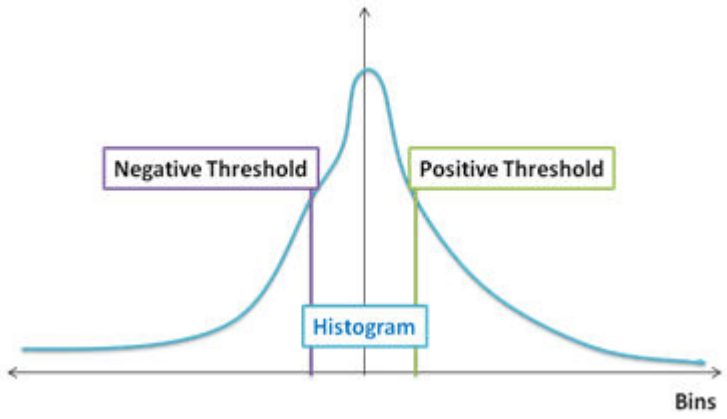

Figure 4: Histogram Based Thresholding

2.3.2 Elimination of shadows

The quality of the processed change map may be severely degraded by the appearance of shadows. Often because of the position of sun during the capture of early and late images, one may have shadows while the other may not. These areas may appear in the initial change map developed from simple differencing as false building changes. Hence it becomes extremely crucial to eliminate errors that occur in with respect to shadows of the objects. To generate the shadows multispectral or RGB images are required.

The shadows in this work were generated as per the Tricolor Attenuation Model-TAM based on the image formation theory (Tian et al. 2009). TAM differentiates between the shadowed regions and those without shadows with respect to the spectral power distribution of daylight and skylight estimated as per the Planck's blackbody irradiance law.

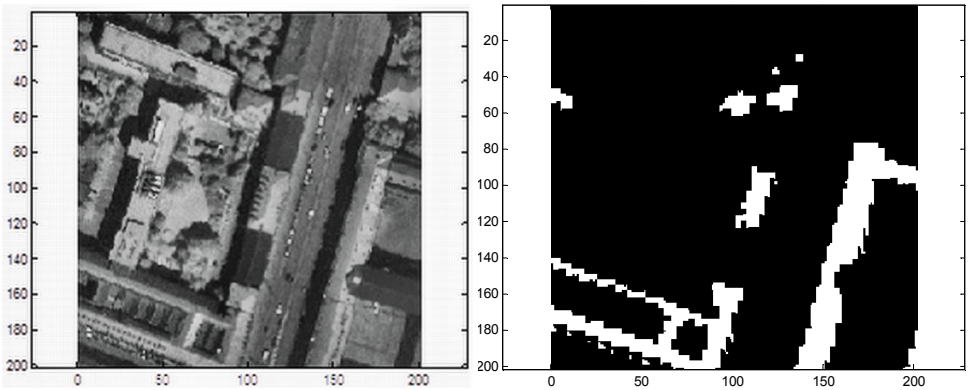

Figure 5: An image section from Munich data set and the respective building shadows

2.3.3 Elimination of the vegetation

Since the object of interest in this study is buildings vegetation changes are unnecessary addendum. To separate the building changes from vegetation changes, it is required to eliminate changes due to vegetation in the initial change map. The elimination of height changes due to vegetation requires availability of multi-spectral images. With the availability of images corresponding to the red and near infra red channels the vegetation in the scene can be detected by evaluating the Normalized Difference Vegetation Index (NDVI). The NDVI is calculated as follows

$$NDVI = \frac{NIR - RED}{NIR + RED} \qquad \text{..... (5)}$$

Where NIR is referred to the near infrared response of the pixel, multi spectral system (MSS) band 4 and RED is the red response i.e. MSS band 2 (Coppin et al. 2004). NDVI would provide the pixels in the image that corresponds to vegetation. Once such information is obtained for both the images a mere difference of this information provides the vegetation change pixels. A mask is prepared from these pixels which correspond to the vegetation changes that may appear in the change map which can be applied to the initial change map which will now only indicate the changes in buildings along with some other errors.

2.4 Secondary change detection

As already explained in previous sections, the quality of the change map obtained from the preliminary stage is still insufficient. The initial change map often suffers from the noise and other errors present in the images and the DSMs. Thus the required refinement is carried out in the secondary change detection. The main objective here is to identify real building change pixels. In the secondary change detection stage pixel gray level information is used from the early and late images to refine the change map.

The secondary change detection stage is implemented within a sliding window algorithm as shown in figure 6, where the optimum window size was decided by testing pixels from both classes i.e. 'no change' and 'change' (see Chapter 4). The sliding window algorithm processes a section of the image predefined within a window and applies the result to a single pixel in this case. Although various methods are available that adapts window sizes according to homogeneity or similarity amongst the pixels in a neighborhood (Patricio et al. 2004). An example is using region growing; the window size can be set according to the size of the region grown. However in this study it was not possible, since different divergence functions provide varying efficiency with window sizes, as was seen from the analysis on the training regions (see Chapter 4.). The initial intake for the sliding window algorithm is the window size, the images and the seed points from the processed DSM difference.

Within the window the marginal and joint probabilities are estimated along with the similarity measures explained further in this section. The obtained metric value from the similarity measures is assigned to the staring pixel in the window. The process is repeated for all the pixels obtained from the initial change map. Afterwards the tradeoff parameter α is estimated to develop the refined change map. Fundamentally, the tradeoff parameter is determined using the mixed information, mutual information and the joint entropy as in equation 22. However in this approach it is determined by combining various information similarity measures (see section 2.4.5).

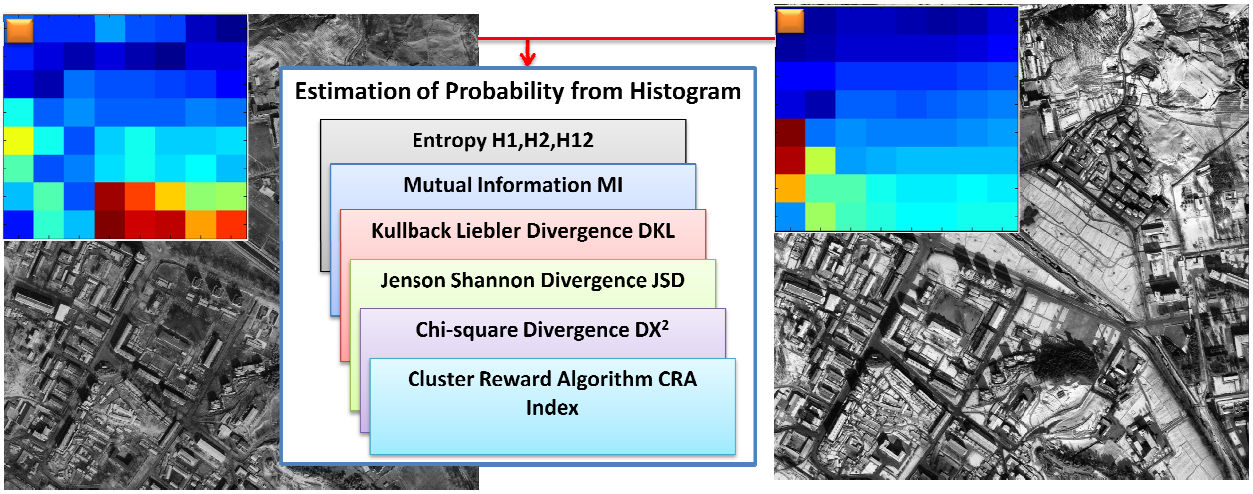

Figure 6: Mechanism of the Sliding Window Algorithm

2.4.1 Probability Density Estimation

In literature there are many approaches for probability density estimation such as parametric, semi-parametric and non-parametric techniques. Bruzzone & Prieto (2002) use a semi-parametric approach for probability density estimation. For simplicity the histograms are used for generating the probability density estimates in this study. The probability estimates can be generated from the histogram as follows

$$P(x) = \frac{1}{N}.\{H(x)\} \qquad \text{..... (6)}$$

Where *H(x)* denotes the histogram of the image, *P(x)* denotes the probability density and N is the sum of all values in the histogram. For the joint probability a joint histogram is required.

Figure 7 and 8 show the individual and joint histograms for the early and late images in the East Asia and the Munich data set. In figure 7a) the histogram for the early image is similar to lognormal however the histogram for the late image has more components than that in the former and the shape is rather unidentifiable. Figure 7 c) shows the joint histogram for the early and late images with a lot of holes. A similar observation is true for the histograms from the images in Munich data set shown in figure 8. With so many holes in the joint histogram, the estimation of similarity measures using PDFs based upon the histogram becomes rather tedious especially in Mutual Information and CRA where a logarithm of the joint PDF is required by replacing all zero values to a minuscule non zero positive value, the logarithm of the joint PDF can be tolerated.

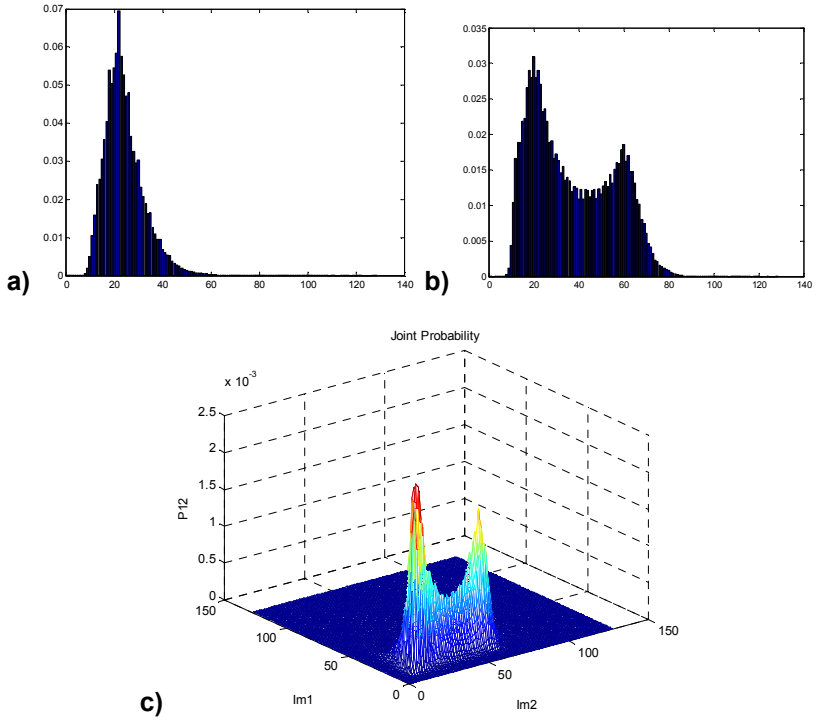

Figure 7: PDE-Probability Density Estimate Dataset 1, - a) PDE Image 1, b) PDE Image 2, c) Joint PDE

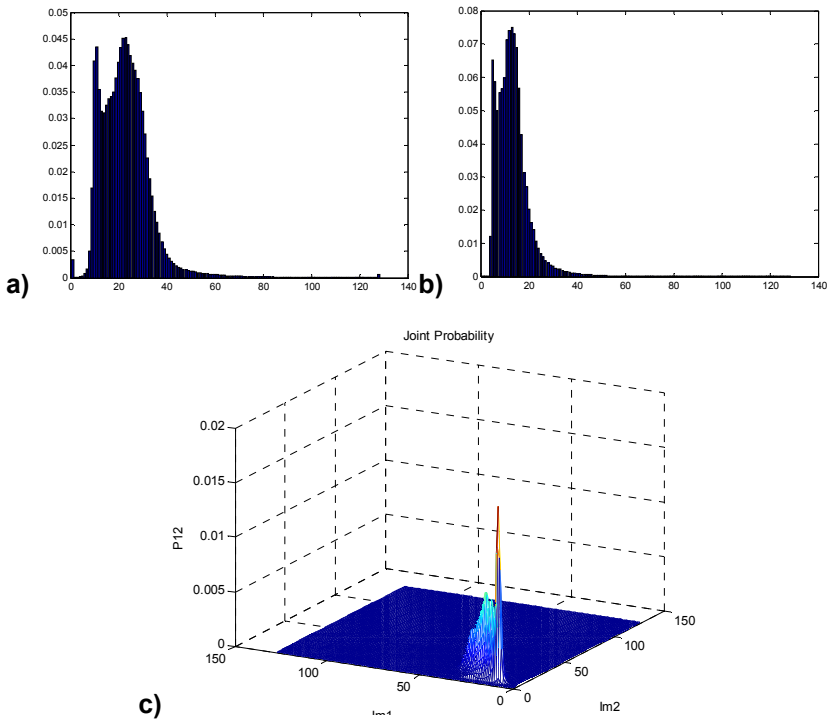

Figure 8: PDE-Probability Density Estimate Dataset 2, - a) PDE Image 1, b) PDE Image 2, c) Joint PDE

2.4.2 Estimation of Information similarity Measures

The concept of similarity is frequently used for classification purposes. In image registration several information similarity measures are regularly used. The gist of using such methods is defining the similarity between two variables by a similarity metric or index which delineates the relationship between them. However there is often uncertainty between the two variables especially when the two variables hold a wide range of values such as that in case of images. In such cases, it is often required to adopt different complicated approaches. Often one similarity measure is not sufficient to characterize the changes. For example the Jenson Shannon divergence usually cause the same effect as over thresholding while the mutual information cause effects similar to under thresholding. Therefore it can be assumed that the combination of two would provide better characterization of changes. The same analogy is followed by certain other information similarity measures. Thus it becomes extremely productive to combine information from several information similarity measures. In literature most similarity measures are based on probability theory. Once the probability density estimate is available the next step is to estimate the information features.

Let $\{I_1, I_2\}$ be the set of early and late images maps a pixel coordinate $x \in R^l$ to intensity $I(x) \in R^k$ where *k = 1*, for panchromatic images and *l = 2* for 2D co-ordinate systems then – $S_c(I_1, I_2) = f(I_1, I_2, c)$ represents the similarity metric with *c* as the criterion for selection. S_c has a maximum value when the two images are identical (Inglada et al., 2004).

a) Joint Entropy

When considering two images simultaneously, a measure of uncertainty associated with them can be defined by the joint entropy. If each pixel in I_1 and I_2 have gray values x_1 and x_2 respectively then the joint entropy $H(I_1,I_2)$ can be defined as follows

$$H(I_1,I_2)=\sum_{x_1}\sum_{x_2}P(x_1,x_2).logP(x_1,x_2) \quad \text{..... (7)}$$

where $P(x_1,x_2)$ represents the joint probability density of the two images. While the individual entropies are defined as follows

$$H(I_1)=\sum_{x_1}P(x_1).logP(x_1) \quad \text{..... (8)}$$

$$H(I_2)=\sum_{x_2}P(x_2).logP(x_2) \quad \text{..... (9)}$$

where $H(I_1)$, $H(I_2)$, $P(x_1)$ and $P(x_2)$ represents the individual entropy and probability density estimate of the two images. It is observed that the joint entropy is always greater than or equal to the sum of the individual entropies.

b) Mutual Information

Mutual information is an important measure in change detection in literature. Erten et al. (2010) and Jahari et al. (2008) use mutual information for change detection. Jahri et al. (2008) estimate the mutual information locally for all the pixels and then use simple thresholding for eliminating those pixels which share less similarity. The accuracy in that case was pertinent to the selection of relevant local thresholds. In information theory mutual information of two images is the quantity that measures the mutual dependence of the two images with respect to their pixel gray values. The mutual information between two images can be formulated as follows

$$I(I_1,I_2)=\sum_{x_1}\sum_{x_2}P(x_1,x_2).log\left\{\frac{P(x_1,x_2)}{P(x_1).P(x_2)}\right\} \quad \text{..... (10)}$$

Mutual information can also be expressed in terms of individual and joint entropy as

$$I(I,I)=H(I_1)+H(I_2)-H(I_1,I_2) \quad \text{..... (11)}$$

If $H(I_1 / I_2)$ and $H(I_2 / I_1)$ defines the conditional entropies for the two distributions, then the mutual information can be formulated as

$$I(I_1, I_2) = H(I_1) - H(I_1 / I_2)$$

..... (12)

$$I(I_1, I_2) = H(I_2) - H(I_2 / I_1)$$

..... (13)

When two variables match completely, from equation 13, it can be observed that $H(I_1/I_2)$ = 0, while the distribution corresponds to discrete data, would mean both the mutual information and the entropy of the distribution are equal. Hence it can be stated that a variable within itself sustains an amount of information that can be matched by any other variable. Figure 9 shows the relation between the marginal, conditional and joint entropy with mutual information.

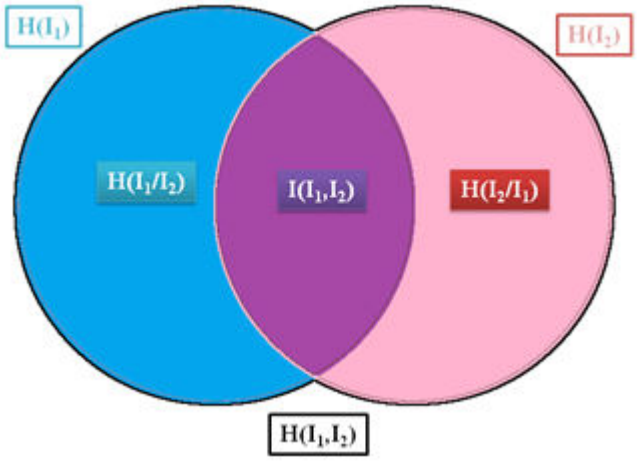

Figure 9: Relation between marginal, conditional and joint entropy with mutual information.

c) Kullback Leibler Divergence

The Kullback Leibler Divergence is one of the most commonly used 'f-divergence' functions. In probability theory, the 'f-divergence' constitutes a set of functions which are used to evaluate similarity between two probability distributions. The Kullback Leibler Divergence (KLD) is a statistical measure that models the resemblance between a candidate probability distribution and a known one. Inglada (2009) use KLD for change detection in SAR images. The Kullback Leibler divergence utilizes only the individual probabilities of the two profiles. Again if P1 and P2 are the two profiles as in section 2.4.1, then Kullback Leibler divergence can mathematically be represented as

$$KLD(I_1, I_2) = \sum_{x_1} P(x_1).log\left\{\frac{P(x_1)}{P(x_2)}\right\}$$

..... (14)

where *KLD* denotes the Kullback Leibler divergence. It has been proved in literature that *KLD ≥ 0*, and non symmetric in nature. *KDL = 0*, if the two distributions match exactly and if they are completely different, it may potentially rise to infinity. The Kullback Leibler divergence of the two distributions can also be expressed in terms of marginal distributions

d) Jenson Shannon Divergence

Jenson Shannon Divergence (JSD) is an extension from KLD. Jensen-Shannon divergence (JSD) gives the measure of variation between two probability distributions, which may well be used to define the similarity between two variables (Grosse et al. 2002). In comparison to KLD, Jenson Shannon divergence always has a finite value. The square root of JSD defines a similarity metric. The JSD is expressed in terms of the marginal probabilities $P(x_1)$ and $P(x_2)$ as follows

$$JSD(I_1, I_2) = \sum_x \left[P(x_1).\log\left(\frac{P(x_1)}{m(x_1, x_2)}\right) + P(x_2).\log\left(\frac{P(x_2)}{m(x_1, x_2)}\right)\right]$$

..... (15)

where $m(x_1, x_2) = \frac{1}{2}\{P(x_1) + P(x_2)\}$.

The Jenson Shannon divergence is bounded by 1, i.e. $0 \le JSD \le 1$.

e) Chi-square Divergence

The chi-square divergence is also one of the divergence functions from 'f-divergence' along with KLD. Mathematically it has a very simplistic formulation, illustrated as follows

$$\chi^{\alpha} = \frac{1}{2}.\left\{\frac{(P(x_1) - P(x_2)^{\alpha}}{P(x_1)}\right\}$$

..... (16)

Where α can attain a wide range of values depending upon the user and application. The simplest case is with α =1; in which case the resulting distance parameter is known as 'total variation distance'. However in most cases this is not sufficient to categories real changes and hence a higher value for α is used. The most commonly used numeric for α is 2 as in this study.

f) Cluster Reward Algorithm

Another method assessing the similarity between two variables is the Cluster Reward Algorithm (CRA). CRA is measure based on the joint and the individual probabilities of two variables just like the mutual information and is mathematically defined as

$$CRA(I_1,I_2) = \frac{\sum_{x} P^2(x_1,x_2) - \sum_{x_1} P^2(x_1).\sum_{x_2} P^2(x_2).}{\sqrt{\sum_{x_1} P^2(x_1).\sum_{x_2} P^2(x_2).} - \sum_{x_1} P^2(x_1).\sum_{x_2} P^2(x_2).}$$

..... (17)

CRA index attains greater values when the joint histogram has little dispersion (Inglada & Giros 2004). Such an observation may exist for a flat histogram or when the image intensities are already clustered within the histogram. Hence it may be possible to predict the values of the other image. A remarkable advantage of using this approach is that the joint histogram noise has a weaker influence (Inglada & Giros 2004).

g) Bhattacharya Distance

The Bhattacharyya distance is a statistical measure that is often used in literature as a class separability measure for feature selection (Choi & Lee 2003). Benedeck et al. (2009) use the Bhattacharyya distance for measuring the local textural dissimilarities. The Bhattacharyya distance can be mathematically formulated as

$$D_{BC} = \sum_{x} \sqrt{\sum P(x_1).\sum P(x_2)}$$

..... (18)

2.4.3 Variational and Mixed Information

Analogous to mutual information another parameter can be defined which unlike the similarity assessment by mutual information, defines the variation between two variables. This is termed to be the variational information (Pagot et al. 2008) represented as follows

$$VI(I_1,I_2) = \sum_{x_1}\sum_{x_2} P(x_1,x_2).log\left\{\frac{P^2(x_1,x_2)}{P(x_1)P(x_2)}\right\}$$

..... (19)

$$VI(I_1,I_2) = H(I_1,I_2) - I(I_1,I_2)$$

..... (20)

The variational information is seen to have an inverse proportionality over mutual information. Hence for the same joint entropy if mutual information increases then variational information decreases. Analogous to the manner in which mutual information is a measure of resemblance

between two variables, the variational information is a measure of independence of two variables (Gueguen et al. 2011). Figure 10 shows the relation between variational information mutual information and joint entropy.

The mixed information is linearly related to mutual and variational information measures defined as follows

$$I_\alpha(I_1,I_2)=(1-\alpha)I(I_1,I_2)-\alpha VI(I_1,I_2) \quad \text{..... (21)}$$

$$I_\alpha(I_1,I_2)=\sum_{x_1}\sum_{x_2}P(x_1,x_2).log\left\{\frac{P^{(1+\alpha)}(x_1,x_2)}{P(x_1).P(x_2)}\right\}$$
$$I_\alpha(I_1,I_2)=I(I_1,I_2)-\alpha.H(I_1,I_2) \quad \text{..... (22)}$$

Where α trades off between mutual information and variational information predominance (Gueguen et al. 2011). The parameter α is defined for the interval [0, 1]. When α = 0, the mixed information is equivalent to mutual information, while for α = 1, the mixed information is equivalent to negative of variational information. On the contrary when $\alpha = I(I_1,I_2)/H(I_1,I_2)$ then I_α=0.

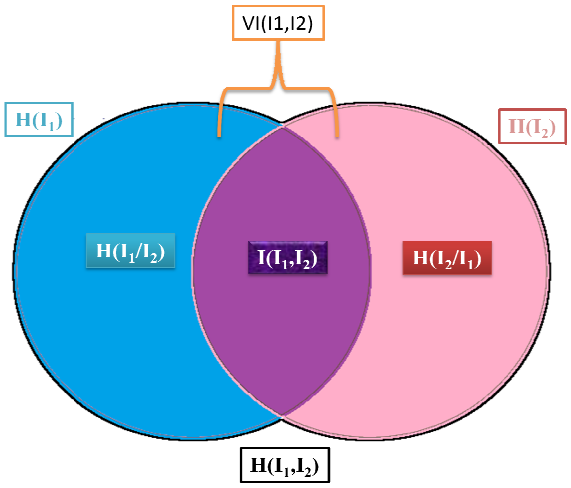

Figure 10: Mutual Information and Variational Information

2.4.4 Selection of the optimum Window size

In order to develop the change map all parameters described before need to be estimated. Also the selection of the optimum window size for estimation of these information measures is crucial. In order to determine the optimum window sizes tests can be performed various training areas manually selected into two classes i.e. 'change' and 'no change' from the thresholded DSM difference. Figure 11 and figure 12 shows the training areas for the two classes in the East

Asia and Munich data set respectively. The tests include estimation of parameters and analysis of the extent to which the parameters are capable of differentiating between the pixels from both the classes. The results from this analysis are illustrated in Section 4.

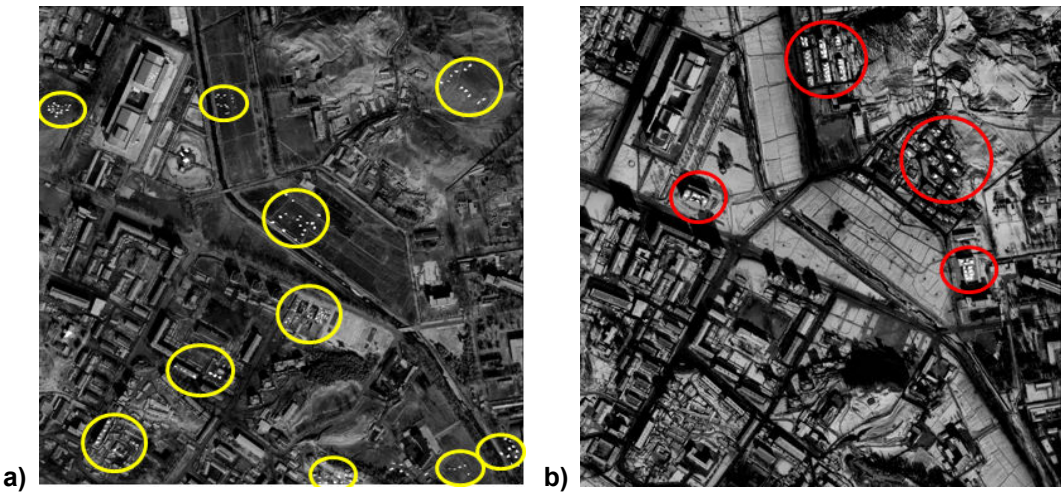

Figure 11: Training Areas East Asia Data Set. a) Change Pixels, b) No Change Pixels

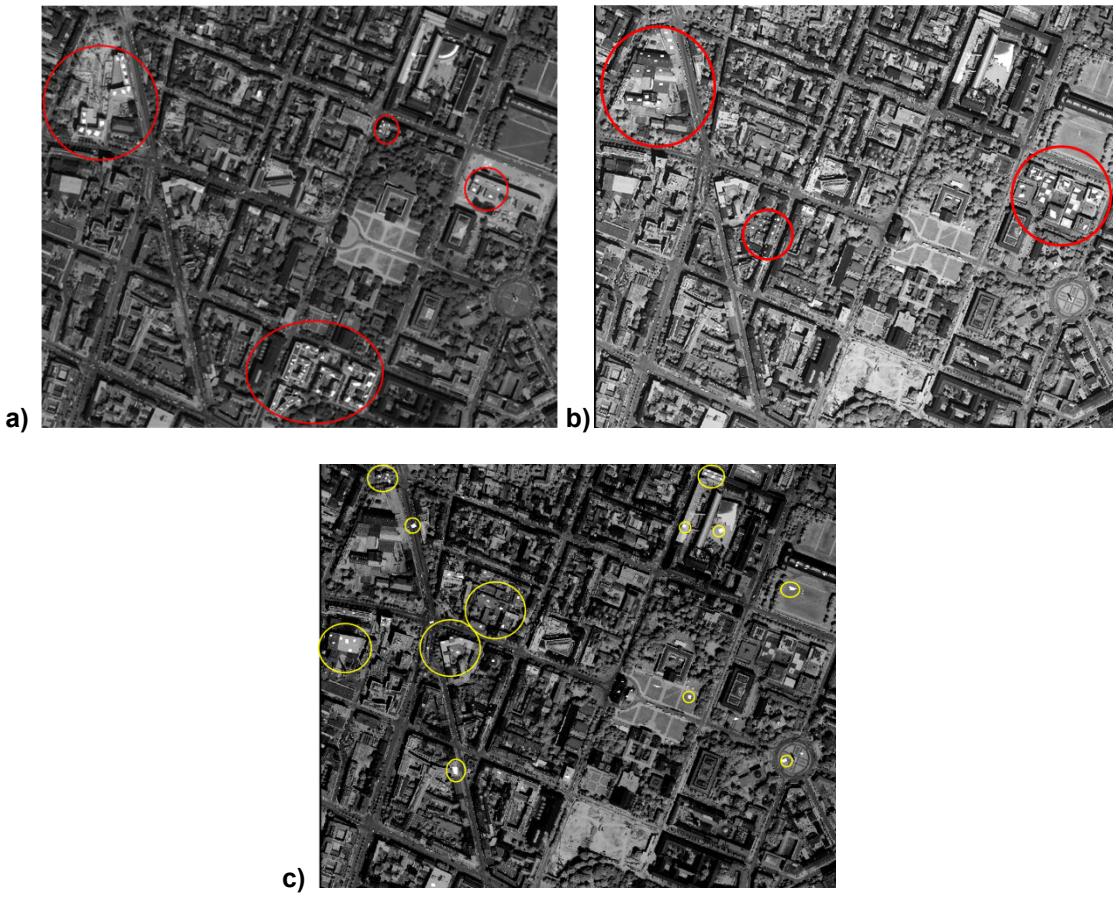

Figure 12: Training Areas Munich Data Set. a) Change Pixels, b) Change Pixels, c) No Change Pixels

2.4.5 Developing the Change Map

The parameter set required for the estimation of the change map is expressed as follows

$$f(I_1,I_2) = [\, I(I_1,I_2), KLD(I_1,I_2), JSD(I_1,I_2), \chi^2(I_1,I_2), CRA(I_1,I_2)\,]$$

..... **(23)**

From equation 22, the tradeoff parameter α is required to be estimated using the different similarity measures instead of mutual information only. From the marginal and joint probabilities α can be directly calculated by using equation 22. Also an efficient way to determine the tradeoff parameter is to use a least squares estimation for equation 23, where the mutual information and joint entropy can be estimated for different window sizes to generate multiple equations (see the modified equation 22 below). The weighted least squares estimation on equation 23 can be iterated such that for the first iteration mixed information is retrieved and for the next one the tradeoff parameter is retrieved. For the second iteration, the normalized parameter $f(I_1,I_2)$ is used instead of mutual information, such that the tradeoff parameter described in equation 22, is determined by combining information from different similarity measures described in equation 23. Furthermore using weighted least squares provides a superior approximation.

From equation 23,

$$I_\alpha(I_1,I_2)_n = I(I_1,I_2)_n - \alpha.H(I_1,I_2)_n \qquad n = 32,40,48,64.$$

it can be seen that the mixed information is a linear combination of mutual information and joint entropy. In order to develop an over determined system of equations based on the above equation, four window sizes are used in the sliding window algorithm (beginning of section 2.4) i.e. $n = 32,40,48,64.$. Since 32x32 seemed to have consistent results in most cases during the training analysis, the selected window sizes were chosen in proximity to 32x32 along with a larger window size of 64 to effectuate a smoothing effect. For each window size the mutual information and the joint entropy is estimated. This gives us 4 equations that generates an over determined system. Now the remaining unknowns are the mixed information and the tradeoff parameter which are estimated using the weighted least squares method, where the weights are estimated using the variances of mutual information. Thus the resultant coefficients obtained from least squares method are the mixed information and the tradeoff parameter. Since in this study one of the objectives is to combine different information similarity measures only the mixed information is retained and the tradeoff parameter is re-estimated in the second iteration.

For the second iteration now only the trade off parameter has to be determined. The above equation is normalized and the normalized similarity measures from the parameter set described in equation 23 are used. Now with 5 different similarity measures ($m = MI_{32}$, *KLD,*

JSD, X^2, CRA), 5 equations are obtained from equation 24 to generate an over determined system, which is solved using the weighted least squares. Again the weights are determined from the variances of the parameters (Similarity measures) in this case. Thus the tradeoff parameter is obtained from the different similarity measures in the parameter set.

$$I_\alpha(I_1,I_2) = m(I_1,I_2) - \alpha.H(I_1,I_2)_{32} \qquad m = MI_{32},KLD,JSD,\chi^2,CRA$$

..... **(24)**

Then the change map is in general is then estimated as follows

$$CD=(1+\alpha).KLD(I_1,I_2)$$

..... **(25)**

2.4.6 Change Map Refinement

The attained change map may still have individual or group of pixels that may not belong to the concerned class of objects in the analysis, which in this case are buildings. These pixels may be removed by using morphological region removal techniques. In this case all the apparent buildings and other objects are labeled and processed individually. Within each object every pixel is checked for connectivity with neighbors and thus total number of pixels appearing in a nexus is estimated. Further then based upon a given maximum region size- $S_{\max}$ the object is eliminated if the size is comparatively lower than $S_{\max}$, otherwise retained. This is more effective than morphological opening since the desired objects are unaffected (see Appendix B).

2.4.7 Accuracy Assessment

The effectuality of any algorithm comes forth only with some means of assessment with factual solidarity. In several cases this assessment can be visual human perception, however for change detection that is insufficient to provide reasonable confidence. Hence a methodical assessment analysis is indispensable for change detection. There are various methods in literature for assessment of change map with respect to reference data. The standard way of evaluating results with respect to reference data is using a pixel based assessment. However often pixel based assessment alone is not sufficient to characterize the efficacy of an algorithm and hence object based assessment is also required. The methods for pixel based and object based assessment within this work are illustrated as follows

a) Pixel Based Assessment.

The pixel based assessment refers pixel wise quality and quantity analysis of the similarity between the developed change map and the reference data. A common and popular method for accuracy assessment is the error matrix or more commonly known as the confusion matrix, which describes the accuracy of the results with respect to a reference data in this case the reference data, explained as follows -

Confusion Matrix

A confusion matrix categorizes the number of pixels assigned to a certain class in the change map with respect to the real changes as delineated in the reference data (Congalton 1991). The rows the number of compared pixels in the change map while the columns represent those in the reference data. The diagonal terms represents the correctly classified pixels, i.e. those which exist in both the change map as well as in the reference data. On the contrary the off-diagonal terms represent the false classifications. A standard way in assessment of change detection is to classify the confusion matrix into four terms (Table 1) that are

1. **True Positive –** The number of pixels in the change map that co-exist within the reference data.

2. **False Positive –** The number of pixels in the change map that do not have corresponding pixels in the reference data.

3. **False Negative –**The number of pixels belonging to the class 'no change' in the change map which corresponds to changed pixels in the reference data.

4. **True Negative –**The number of pixels that belong to the class 'no change' in both the change map and the reference data.

Table 1: Confusion Matrix – Pixel Based Assessment

Reference Data / Resultant Change Map	Change	No Change
Change	*True Positive – TP*	*False Negative – FN*
No Change	*False Positive – FP*	*True Negative – TN*

These terms are further used to define certain quality measures which quantify the suitability of the approach under evaluation. These quality measures are defined as follows

1) Branching Factor

The branching factor represents the rate at which the incorrect pixels are classified by the algorithm as changes. It is the ratio of 'False Positive' and 'True Positive',

$$BF = FP/TP \qquad \text{..... (26)}$$

A smaller branching factor signifies good results.

2) Miss Factor

The miss factor represents the rate at which the change pixels in the reference data are missed by the algorithm in classification. It is the ratio of 'False Negative' and 'True Positive',

$$MF = FN / TP \quad \text{..... (27)}$$

The smaller the miss factor the better the results.

3) Completeness

Completeness defines the aerial spread in which the accuracy is 100% or in other words it is the proportion of the total number of correctly classified changed pixels to the total number of changed pixels in the reference data. It is a quantity measure.

$$Completeness = 100.\left\{\frac{TP}{(TP + FN)}\right\} \quad \text{..... (28)}$$

Correctness unlike completeness is a significant quality measure. It is the fraction of total number of pixels correctly identified by the algorithm as changed pixels to the total number of changed pixels in the reference data. As its name, this qualitative measure shows the correctness of the change detection.

$$Correctness = 100.\left\{\frac{TP}{(TP + FP)}\right\} \quad \text{..... (29)}$$

The ideal values for *completeness* and *correctness* are achieved when *FN = 0* and *FP = 0* respectively; in this case both of them are 100%.

4) Quality Percentage

The quality percentage provides for an accuracy measure that combines both completeness and correctness. Ideally it should be 100%. It is defined as the proportion of pixels correctly classified from the total of number of changed pixels in the reference data and the number of wrongly classified changed pixels.

$$QP = 100.\left\{\frac{TP}{(TP + FP + FN)}\right\} \quad \text{..... (30)}$$

The overall accuracy is the defined as the ratio of the total number of correctly classified pixels to the total number of pixels existing in the confusion matrix. Since this measure defines qualitatively accuracy for all the classes in the confusion matrix, it may be very high, even though one of the classes suffers adversely in classification. Hence it is suggested to account for other quality assessment parameters for accuracy assessment as well, since overall accuracy alone may create ambiguity.

$$OA = 100.\left\{\frac{TP + TN}{\left(TP + TN + FP + FN\right)}\right\}$$

..... (31)

Unlike overall accuracy that only takes into account the diagonal elements for the ratio in the numerator, Kappa accuracy considers the non-diagonal elements. It is thus a measure of overall agreement for the confusion matrix. The Kappa accuracy is determined as follows –

$$\kappa = \frac{\rho_0 - \rho_e}{1 - \rho_e}$$

..... (32)

Where $\rho_0 = \sum X_{ii} / N$, X_{ii} is the diagonal element in the confusion matrix, $\rho_e = \sum X_{i+}.X_{+i} / N$, X_{i+} X_{+i} are the marginal total of row i and column i and N is the total number of observation in the confusion matrix.

b) Object Based Assessment.

Object based assessment refers to evaluation based on the detected objects, in this case building in the developed change map with respect to those in the reference data. In this case the confusion matrix is based on objects instead of pixels. An example is shown in table that enlists the various outcomes and reference information for object based change detection.

Table 2: Object Based Assessment

BUILDING	No.
Total Buildings in Reference Data	Nr
Total Buildings in Change Map	Nc
True Changed Buildings in Change Map	Ntc
Missing Changed Buildings	Nm
Unreal Changed Buildings	Nu

1. **True Positive –** The number of buildings in the change map that co-exist within the reference data.

2. **False Positive –** The number of buildings in the change map that do not have corresponding buildings in the reference data.

3. **False Negative –**The number of buildings belonging to the class 'no change' in the change map which corresponds to changed buildings in the reference data.

4. **True Negative –**The number of buildings that belong to the class 'no change' in both the change map and the reference data.

Table 3: Confusion Matrix - Object Based Assessment

Reference Data / Resultant Change Map	Change	No Change
Change	*True Positive – Nd*	*False Negative – Nm*
No Change	*False Positive – Nu*	*True Negative – N-Nd*

When the confusion matrix for the object based assessment is available, the quality measures used for analysis in pixel based assessment can be used in a similar way for object based assessment.

3. STUDY AREA AND USED DATA

3.1 Study Area

In this research, two study areas are considered from Eastern Asia and from Munich central area in Germany. The test site in Asia has considerably undergone infrastructural development from before as delineated via the captured images from IKONOS-2. Since both the early and late images in this case are provided from the same satellite this data set was expected to illustrate comparatively better results in detecting building changes. However it was further noted that the appearance of snow the late acquired image could result in identification of false building changes, as the early image is devoid of snow. Also for the Munich central area at hand, two data sets from IKONOS-2 and WORLDVIEW-2 respectively as the early and late captured images were used. Further details on the data sets are provided in Table 3 while the respective details of the two satellites from which the images were captures are provided in Table 4. The Eastern Asia data set comprises of a 1000x1000 pixels which geographically 1km^2, while the Munich data set comprises of 2500x2500 pixels that geographically corresponds to approximately 6 Km^2. Similar to the Asia site this study area also clearly depicts building changes. Clearly evident are the demolished and reconstructed buildings in the central area.

Table 4: Datasets and Sources

Test Data Set	Image Size (pixels)	Satellite	Year (Early | Late)
Eastern Asia	1000x1000	IKONOS -2 | IKONOS -2	2006 | 2010
Munich	2500X2500	IKONOS -2 | WORLDVIEW -2	2005 | 2010

Table 5: Satellite Details

Characteristic	**IKONOS - 2**	**WORLDVIEW - 2**
Date of Launch	September 1999	October 2009
Orbit Height	681-709 km	770 km
Orbit Type	Sun Synchronous near polar	Sun Synchronous
Repeat Cycle	14 days max	1.1 days
Panchromatic Resolution	1m	46 cm
Multispectral Resolution	4m	1.85 m
Channels	4	8
Swath Width	13-70 km	16.4 km
Sources	*ESA Earthnet online*	*Digital Globe*

3.2 Test Data

Stereo optical images were used from high resolution satellites to generate the DSMs used in the proposed method. The raw optical images were processed for radiometric and stereo corrections. The images were ortho-rectified and co-registered to sub-pixel level accuracy before being used to evaluate the algorithm. Since the Munich data set is very large to process a section of 900x1100 pixels is selected, which includes most building changes in the Munich data set for the evaluation analysis. Figure 13 and figure 14 show the respective early and late images for the two data sets. Figure 15 shows the 900x1100 section of images used for the experiments from Munich data set.

Figure 13: East Asia test data site area. Left: Early Image, Right: Late Image

Figure 14: Munich test data site, Left: Early Image, Right: Late Image.

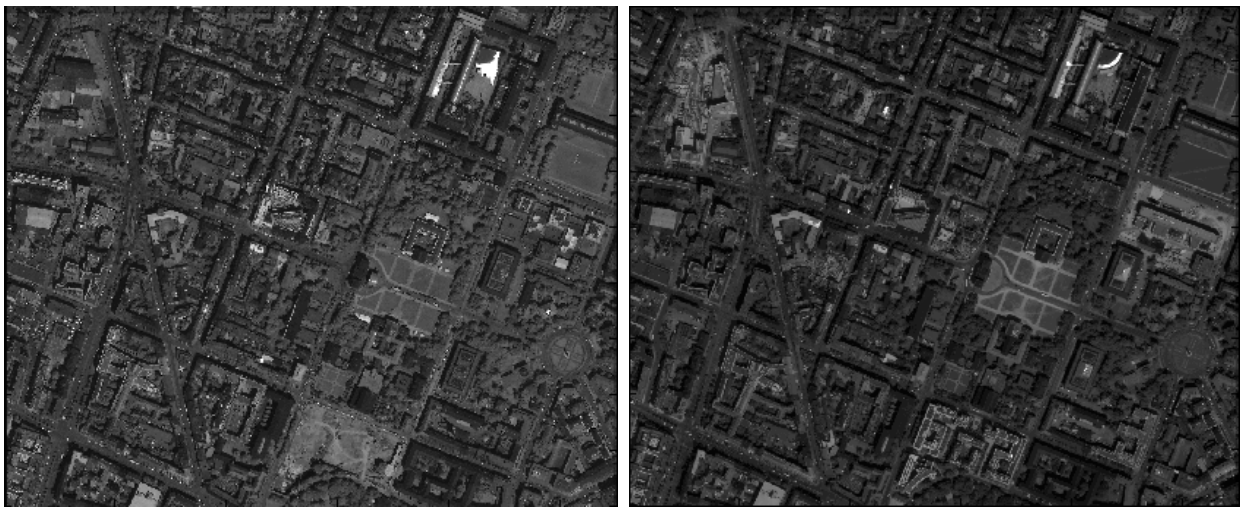

Figure 15: Image Sections used for Experiments from the Munich data set. Left: IKONOS-2 Image (early image), Right: WORLDVIEW-2 Image (late image)

3.3 DSM Generation

Several automatic image matching models are available for DSM generation. Some of these are available in XDIBIAS. XDIBIAS is a generic tool used for image processing and evaluating remote sensing data. The accurate reconstruction of small objects from high resolution stereo images needs dense stereo matching algorithms. Such results are rarely achieved with mere correlation of image windows. Semi global matching (SGM) is one such algorithm (Hirschmueller, 2008).

When a single pair of stereo images is at hand, SGM may still result in several outliers. d'Angelo (2010) illustrates an approach to for detection and removal of these outliers. Even after using dense and robust matching algorithms, the generated DSM often has missing information termed usually as 'holes'. The holes occur due to the variation in image contrast and stereo image acquisition. Small holes are filled by either using the height information from the neighborhood with SRTM data. However, for others SRTM data is used. Although the holes are filled manually, the filling may fail in real scenarios. The quality of the DSMs generated from SGM with optical stereo imagery is not as good as that of LIDAR DSMs. The quality also depends upon the resolution of the images..

Figure 16 shows the Technical University Munich building at Arcisstrasse from Munich Data set and its corresponding DSMs in the early and late image. Although not clear by visual interpretation in figure 16b), the DSMs have additional noise of 'salt & pepper' nature, which thus requires supplementary change detection procedure. The height distribution profile in one of the rows and one column are plotted in figure 16, which shows a drastic change for the late image DSM (16 e and f, green curve).

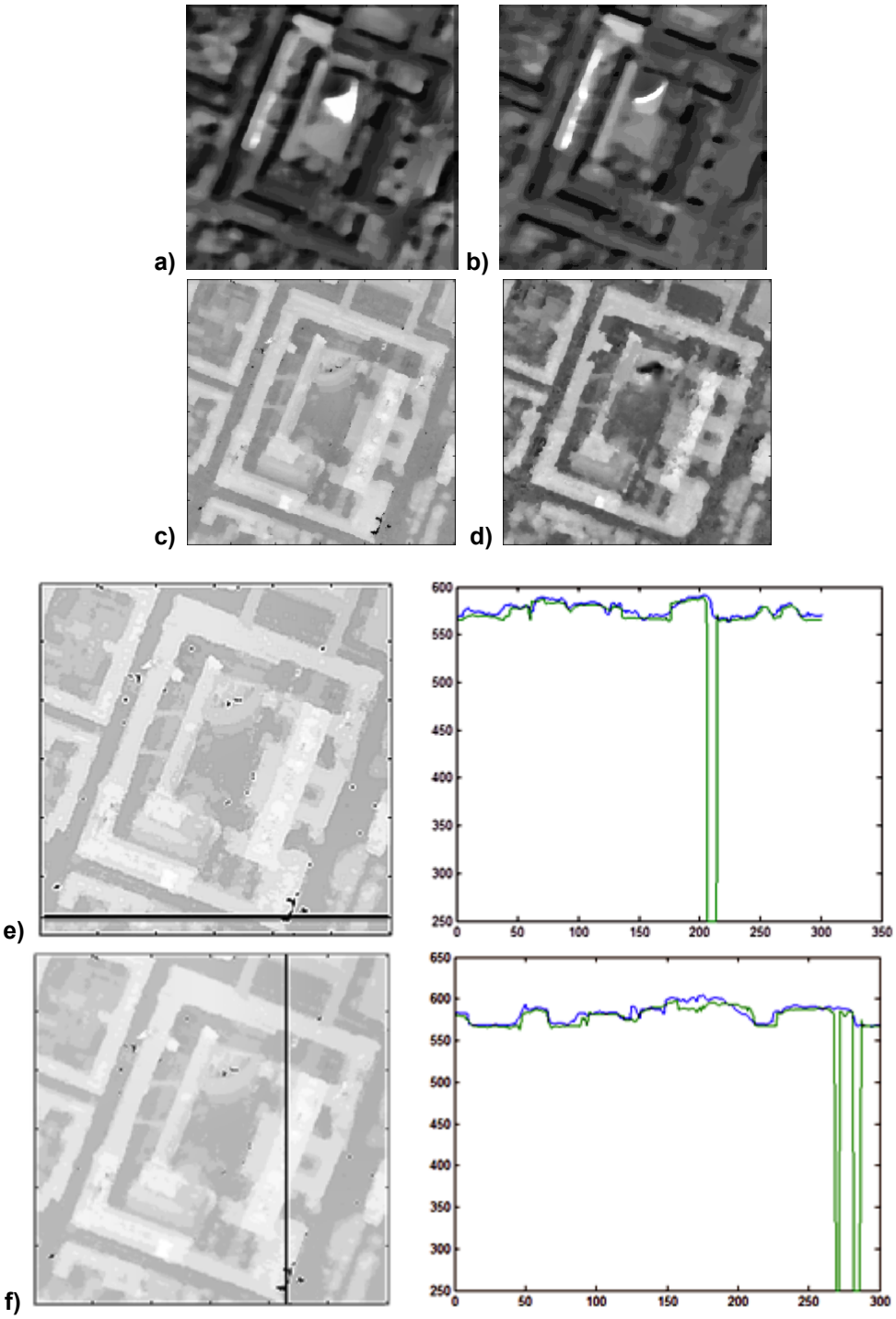

Figure 16: a) TUM building in the late image (WORLDVIEW-2), b) TUM building in the early image (IKONOS-2), c) DSM for the late image, d) DSM for the early image, e) Noise in the DSM for Late image and corresponding height profile for a row of pixels. f) Noise in the DSM for early image and corresponding height profile for a column of pixels.

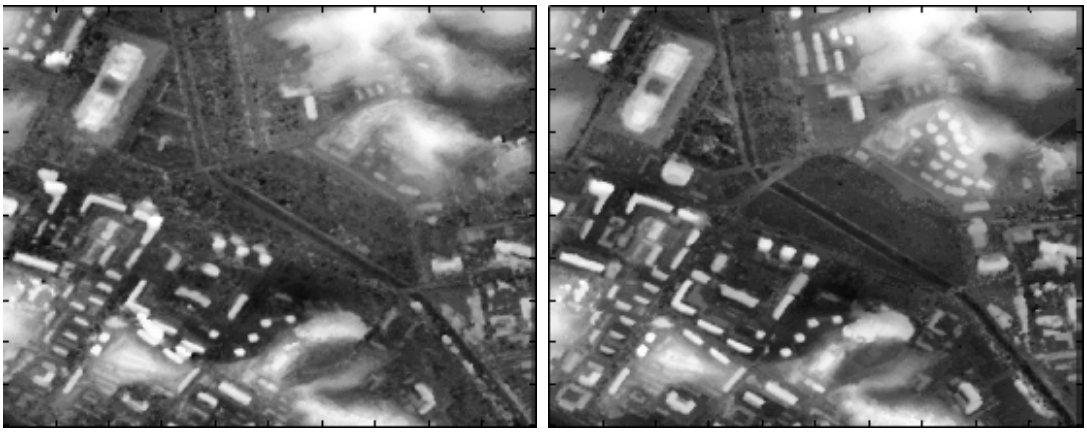

Figure 17: DSMs for East Asia data set. Left: IKONOS-2(early acquisition), Right: IKONOS-2(Late acquisition)

Figure 18: DSMs for Munich data set. Left: IKONOS-2(early acquisition), Right: WORLDVIEW-2(Late acquisition)

Figure 17 shows the DSMs for both images in East Asia data set while figure 18 shows the same for Munich data set. From figure 17 a) and b), the clouds are clearly visible.

3.4 Reference Data

The reference data or 'Ground Truth' not only acts as a reference to evaluate a method but it also acts as a possible way to generally ascertain the suitability and efficiency of a method. It also provides a general idea of the thresholds applied in the method based on careful observation.

The reference data was prepared by visual interpretation of the pre-processed early and late images in case of both the data sets. The preparation involves careful observation of all sections on the images for deciding on existent change. Since this process is done entirely by visual analysis, repeated observation of images is required to be certain of real changes. Certain areas which seem dubious for judgment are classified as no change pixels. Hence the

reference data purely contains pixels which certainly indicate a valid positive or negative change by visual perception. However the reference data is generated as a binary mask which classifies the changes pixels with value “1” and the pixels that have not changed as “0”. Unlike the Munich data set, the East Asia data set had almost negligible negative changes and hence the focus was concentrated towards positive changes alone. Figure 19 shows the reference data for the respective data sets.

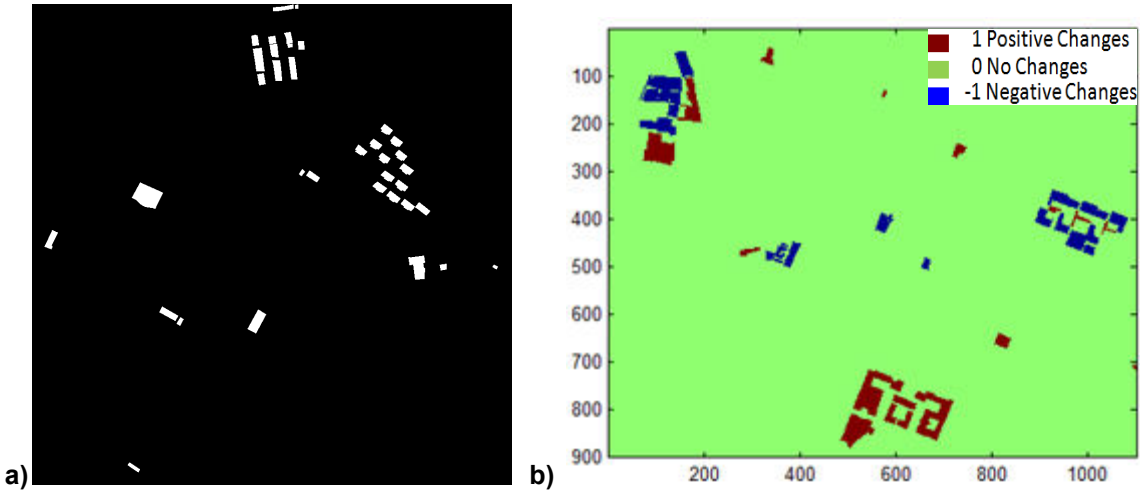

Figure 19: a) Reference data for the East Asia Data Set, b) Reference data for the Munich Data set with the negative changes delineated in blue and the positive changes in red.

For the Munich Data set, it was noticed that certain buildings were partly constructed or existed in the early image and apparently they were reconstructed or modified in the late image. Such buildings were considered in both the change masks i.e. for positive and negative change. For evaluation, a tertiary mask was generated from a mere difference of the two masks such that the common pixels in two masks are set to “0” while the ones corresponding to negative changes in blue with magnitude ‘-1’ and the ones corresponding to positive changes in red with magnitude ‘1’ (see figure 19b). This provided us with reference data for accurate analysis of the changes.

4. EXPERIMENT & RESULTS

In the experiments, the previously explained approach in the workflow in Chapter 3 is applied for the proposed for building change detection in urban areas using the images and the DSMs generated using the HRSS images for the two data sets. Firstly the DSMs are subtracted and thresholded as per section 2.3.1. Then the shadow mask and the vegetation masks are applied to the thresholded DSM difference to eliminate erratic influences due to shadows and vegetation. Again the vegetation masks are derived from the available multispectral images by calculating the NDVI difference between the early and late acquisition. Since there was relatively no vegetation changes in the East Asia data set the obtained vegetation mask was simply a matrix of the size of the panchromatic image with each pixel value as'1'. Figure 20 a) and b) shows the NDVI for the early and late acquisition images for the Munich data set and the respective vegetation mask applied to the Munich data set. Figure 20 c) shows the NDVI difference calibrated to indentify the vegetation changes. The NDVI values in range of 0.3 to 0.7 usually correspond to vegetation and in figure 20 c) these values are retained while the others are set to 0. Figure 20 d) represents the binary vegetation mask which can be applied to the DSM difference and the image difference by a simple arithmetic product.

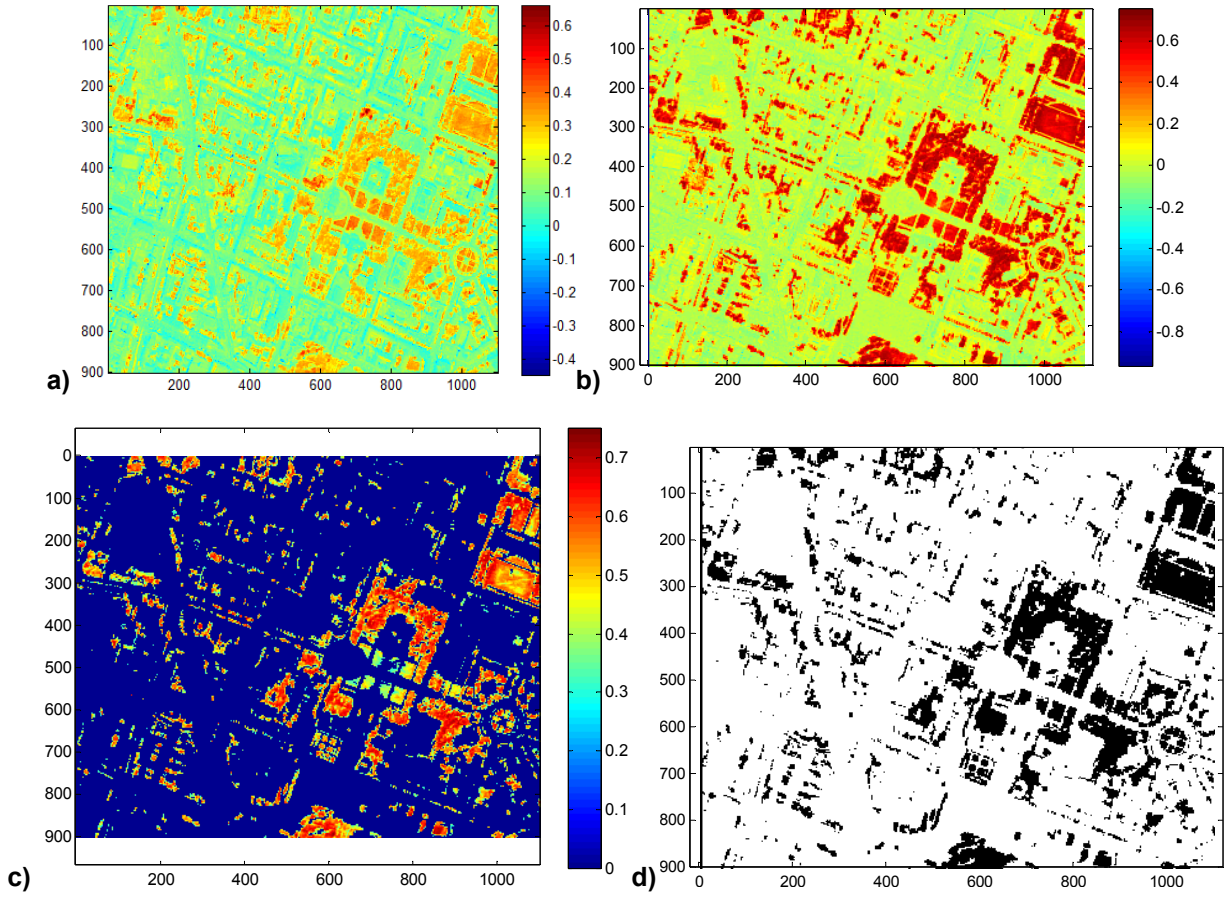

Figure 20: Munich Data Set: a) and b) NDVI for the early and late acquisition respectively. c) Respective NDVI difference calibrated for identifying vegetation changes, d) Binary vegetation mask

Once the shadows and vegetation masks are applied to the DSM difference, the initial change map is obtained as an intermediate result in the method. Figure 21 and 22 shows the DSM difference and the initial change map for the two data sets. Figure 21 only entails the positive changes. Greater the brightness, greater the height difference as can be seen with the colorbar in figure 21. Unlike the East Asia data set the Munich data set entails both positive and negative changes as seen in figure 22. The brighter regions indicate negative changes while the darker ones indicate the positive changes, again this can be inferred from the colorbar in figure 22. From figure 21 and 22, it can be realized that the East Asia data set has clusters of small changed buildings which may actually be residential houses. While the Munich data set comprises of groups of larger changed buildings with in which some part of the buildings may have undergone reconstruction or renovations. The co-ordinates of all non-zero pixels in the DSM difference were stored in a vector which was further used as seed for the secondary change detection procedure.

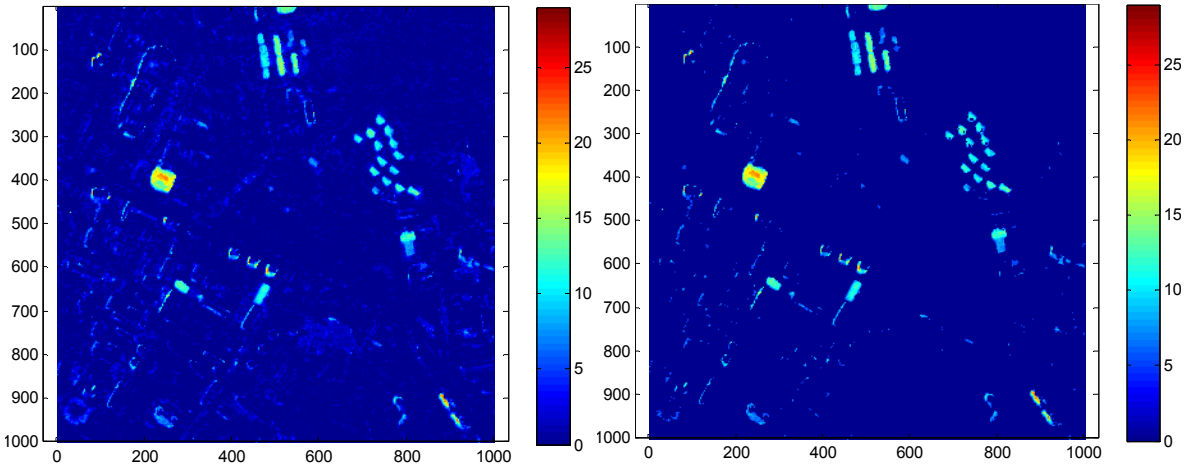

Figure 21: East Asia Data set: Left: DSM difference, Right: Initial Change map

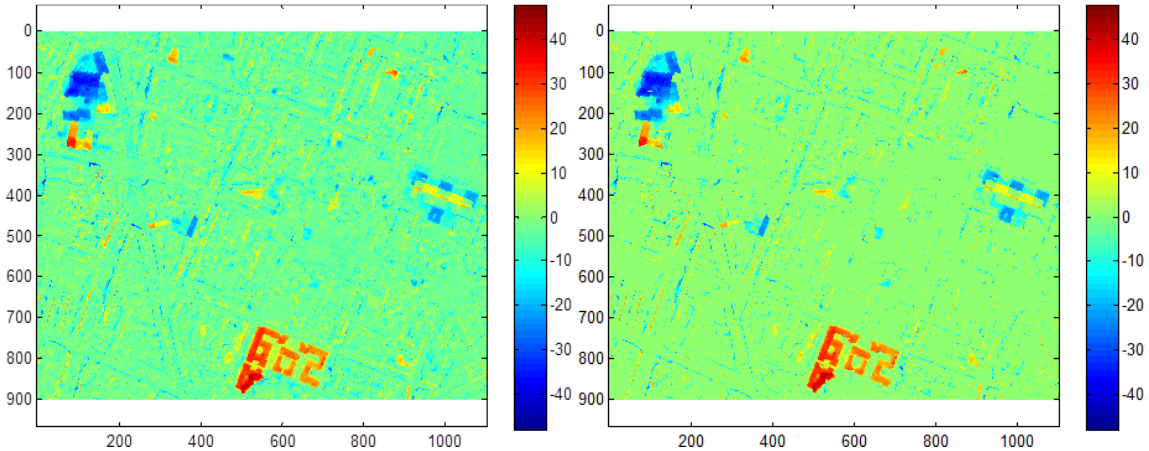

Figure 22: Munich data set - Left: DSM difference, Right: Initial change map

In figure 22 a lot of skeletal structures are seen apart from those which corresponds to buildings. These structures arise from the different resolutions of the early and late images using which the two DSMs were generated with semi-global matching method. Hence the edges of the buildings in the IKONOS-2 DSM corresponding to the early image appears blurred and when this is differenced from the DSM from the late image the edges appear in the difference map as distinct changes. Since these edges attain high magnitude values, thresholding alone is insufficient to eliminate them. As a result for the secondary change detection there is a greater number of pixels to be processed. For correct pixel based assessment, the two reference data were generated enlisting negative changes and positive changes from the early and late images respectively. For assessment, the two reference data was subtracted to obtain a master reference data for comparison with the change map.

It is to be noted that certain buildings appeared in both the early and the late images at their respective positions, however different in shape and size in particular the one in Gabelsbergerstrasse Munich shown in Figure 23. Figure 23 a) shows the changed building in the early (IKONOS-2, 2005) and late image (WORLDVIEW-2, 2010). In figure 23b) the histogram for gray values is shown for the early and late images. Figure 23c) and d) shows the variation in the height as marked in the DSMs for the early and late images in blue and green respectively. It is apparent that there are sharper changes in the DSM for the late image, in which the building edges can be identified easily based on height change as compared to the DSM for the early image. Hence the reproduction of such images was very complicated in the developed change map.

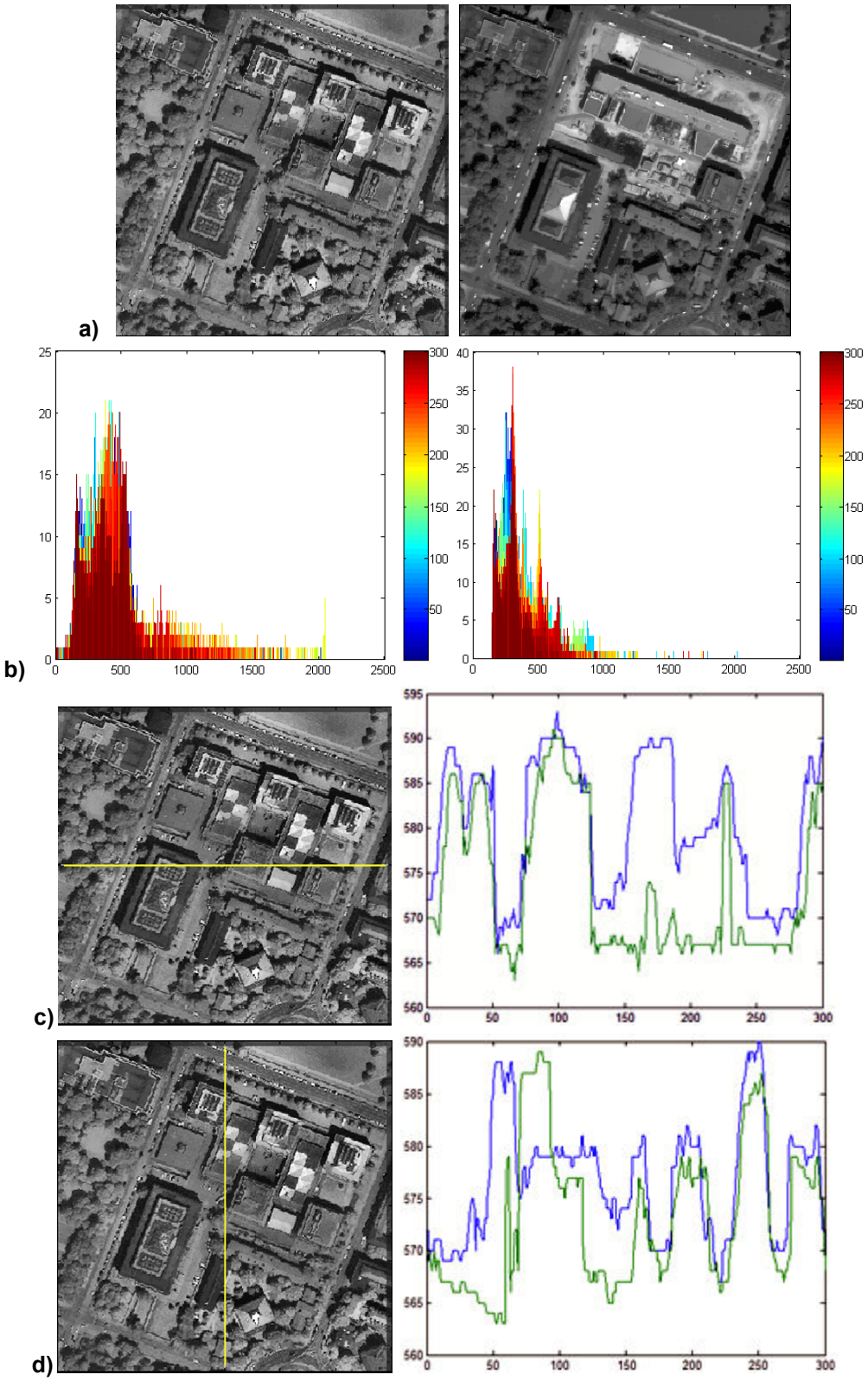

Figure 23 Building at Gabelsburger Strasse Munich, a) Early Image from IKONOS-2, and Late Image from WORLDVIEW-2 section of the building, b) Histogram for the building section in the early and late image, c) & d) DSM variation in early and late image across the shown line.

In the secondary change detection stage a sliding window algorithm was used as mentioned in section 2.4. In order to assess the efficiency of the information similarity measure and suitability of the specific window size, analysis was performed with training areas within the two data sets for both the changed and non changed pixels corresponding to the object buildings. The analysis was simply based upon estimating the parameters in the parameter set $f_{ch}(x_1,x_2)$ and $f_{nch}(x_1,x_2)$ from equation 23. Where $f_{ch}(x_1,x_2)$ represents the parameter set for changed pixels in the training areas and $f_{nch}(x_1,x_2)$ represents the parameter set for unchanged pixels in the training areas. Then by plotting the each corresponding parameter from $f_{ch}(x_1,x_2)$ and $f_{nch}(x_1,x_2)$ together simultaneously a general idea to the efficacy can be obtained. Figure 24 shows such an example. In figure 24 a) the response of the Bhattacharya distance is shown where the blue curve delineates Bhattacharya distance for the unchanged areas, while the green curve represents Bhattacharya distance for the changed areas in the training regions. Figure 24 b) shows a similar plot for the Jenson Shannon divergences. It is to be noted that the plots in figure 24 are evaluated with a window size of 32x32. In the same all the parameters in equation 23 were tested with different window sizes.

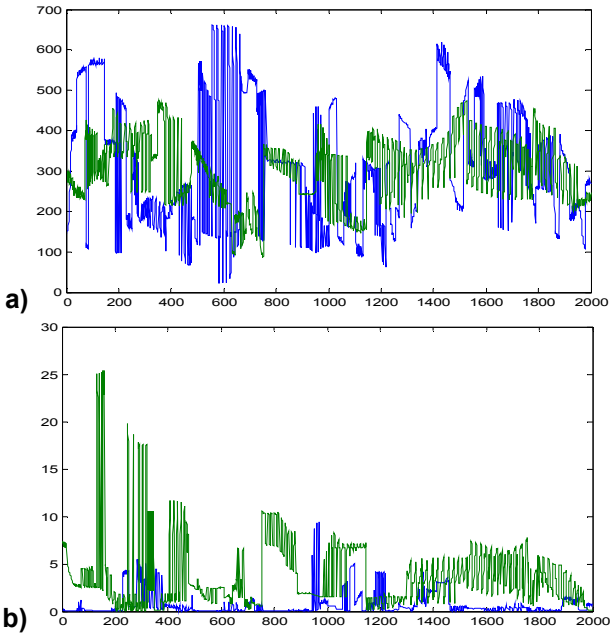

Figure 24: a) Bhattacharya Coefficient, b) Jenson Shannon Divergence

Based on the observations from the training analysis the following points were noted–

- The optimum window size for calculation of the information features was found to be 32x32 for the East Asia data set and was also selected the same for the Munich Data set to save computational efforts.
- The Bhattacharya Distance was found to be an insufficient metric for change classification with the data at hand and hence was eliminated from the analysis.

- In general it can be assumed that lower window sizes such as 21x2 are acceptable for Jenson Shannon Divergence and Chi-square Divergence while for mutual information, Kullback Leibler Divergence and Cluster Reward Algorithm higher window sizes such as those greater than 21x21 are acceptable.
- The selection of a larger window size results in a similar effect to that of pixilation in videos. This results in more change detection than real, however because of the pixilation effect thresholding is possible. With smaller window sizes many false building changes are detected amongst real changes.

Following figures delineate the distribution of the individual parameters from those in the parameter set mentioned in equation 23 for both data sets.

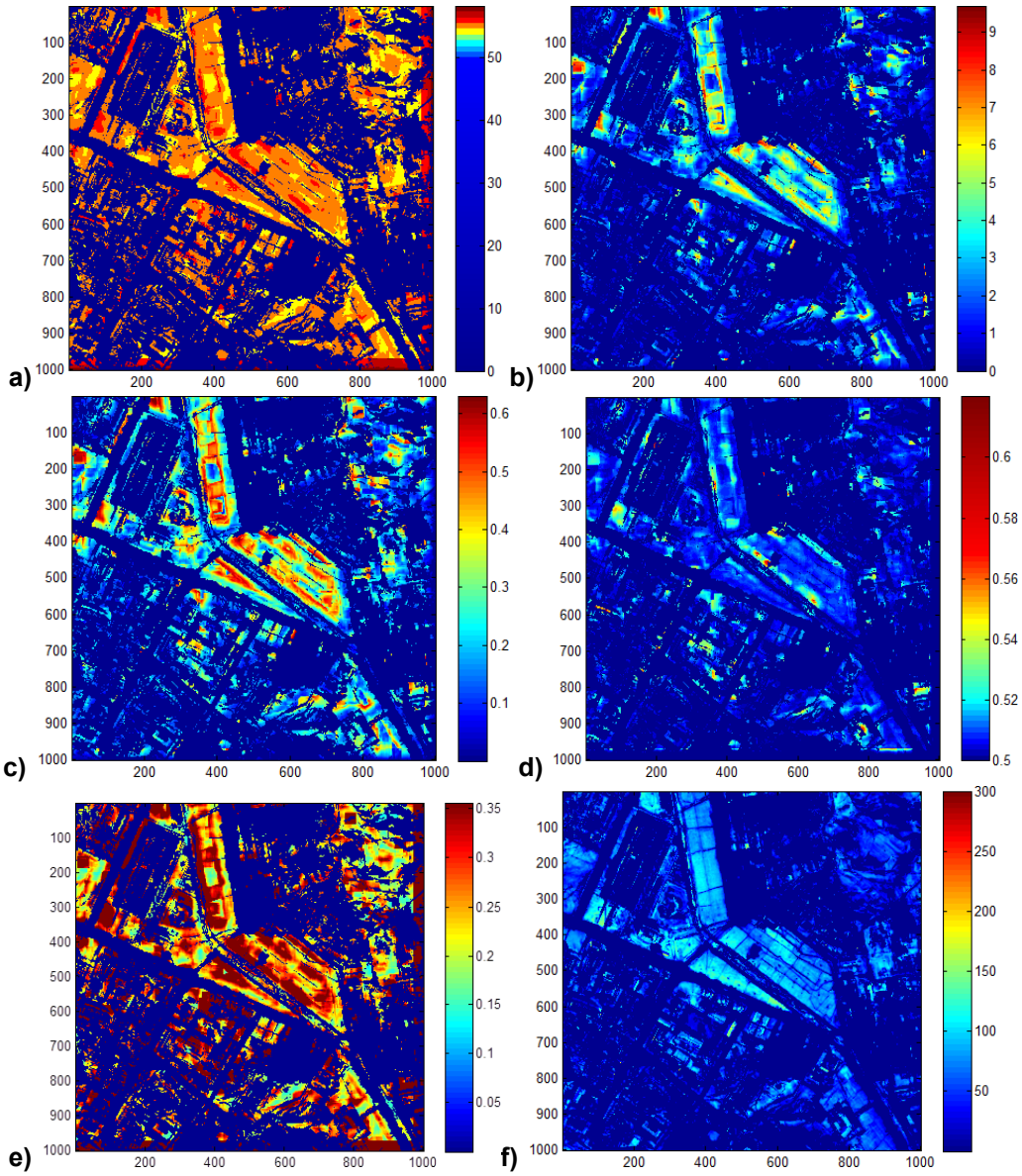

Figure 25: East Asia Data Set with seed from nonzero pixels of processed Image difference- a) Mutual Information, b) Kullback Leibler Divergence, c) Jenson Shannon Divergence, d) Chi-Square Divergence, e) Cluster Reward Algorithm Index, f) Image Difference

Figure 25 shows the obtained profile for the various information similarity measures mentioned in equation 23 in the East Asia data set with the seed taken from the processed image difference in the preliminary change detection. It is to be noted that the processed image difference simply refers to the initial change map developed from the image difference following the steps in preliminary change detection. From figure 25, it can be noted that none of the divergence functions are capable of differentiating between real building changes and false building changes. As already mentioned in chapter 3, the early and late images for East Asia data set were acquired respectively in summer and winter season. In the late image the reflectivity or the gray value in the image is relatively very high compared to the first image. Thus the image difference creates a high difference almost throughout the image in areas influenced significantly by snow. Even thresholding the individual profile will not result in any successful developments, since in this case most changed buildings will get filtered by thresholding. Thus 2D change detection without the DSMs is extremely unreliable in this case, and hence incorporation of information from the DSMs is inevitable in such a scenario for accurate change detection.

Figure 26 shows the obtained profile for the various information similarity measures mentioned in equation 23 in the East Asia data set with the seed taken from the processed DSM difference in the preliminary change detection. Again the processed DSM difference refers to the initial change map developed from the DSM difference by following the preliminary change detection steps. From figure 26 a), the mutual information has a smooth profile for cluster of changed buildings however certain noise is also detected. This noise could well be attributed to the holes in the joint probability distribution. Therefore using the histograms for probability density estimation is often not recommended, however it is frequently due to its simple approach. With respect to the noise the Kullback Leibler Divergence provides the best proximity to reference data. Again if KLD was to be thresholded then the cluster of changed buildings would only be partially reproduced. Similarly the thresholding would be inefficient in case of mutual information since the apparent noise has almost the same magnitude as that of the changed buildings.

Figure 27 shows the obtained profile for the various information similarity measures mentioned in equation 23 in the Munich data set with the seed taken from the processed image difference in the preliminary change detection. Again it can be seen that there are a lot false building changes detected mostly due to the difference in resolution of the early and late acquired images from IKONOS-2 and WORLDVIEW-2. Several straight lines can be seen in the developed profiles in figure 27. These represent the edges of the unchanged buildings and roads or pathways. It is evident that with the incorporation of information from the DSM the falsely detected changed buildings are mostly eliminated in figure 28. However the errors due to the resolution difference in unchanged building edges and roads can still be seen. Also in certain regions such as in mutual information and CRA there are plenty of visible dark red spots. These spots are present due to the holes in the joint probability distribution. Again the mutual information shows the most proximity to the reference data by visual inference. However in comparison to the Chi-Square divergence it also incorporates more noise. This makes way to the approach followed in chapter 3 i.e. determination of a tradeoff parameter to characterize the change map by combining the various information similarity measures in equation 23.

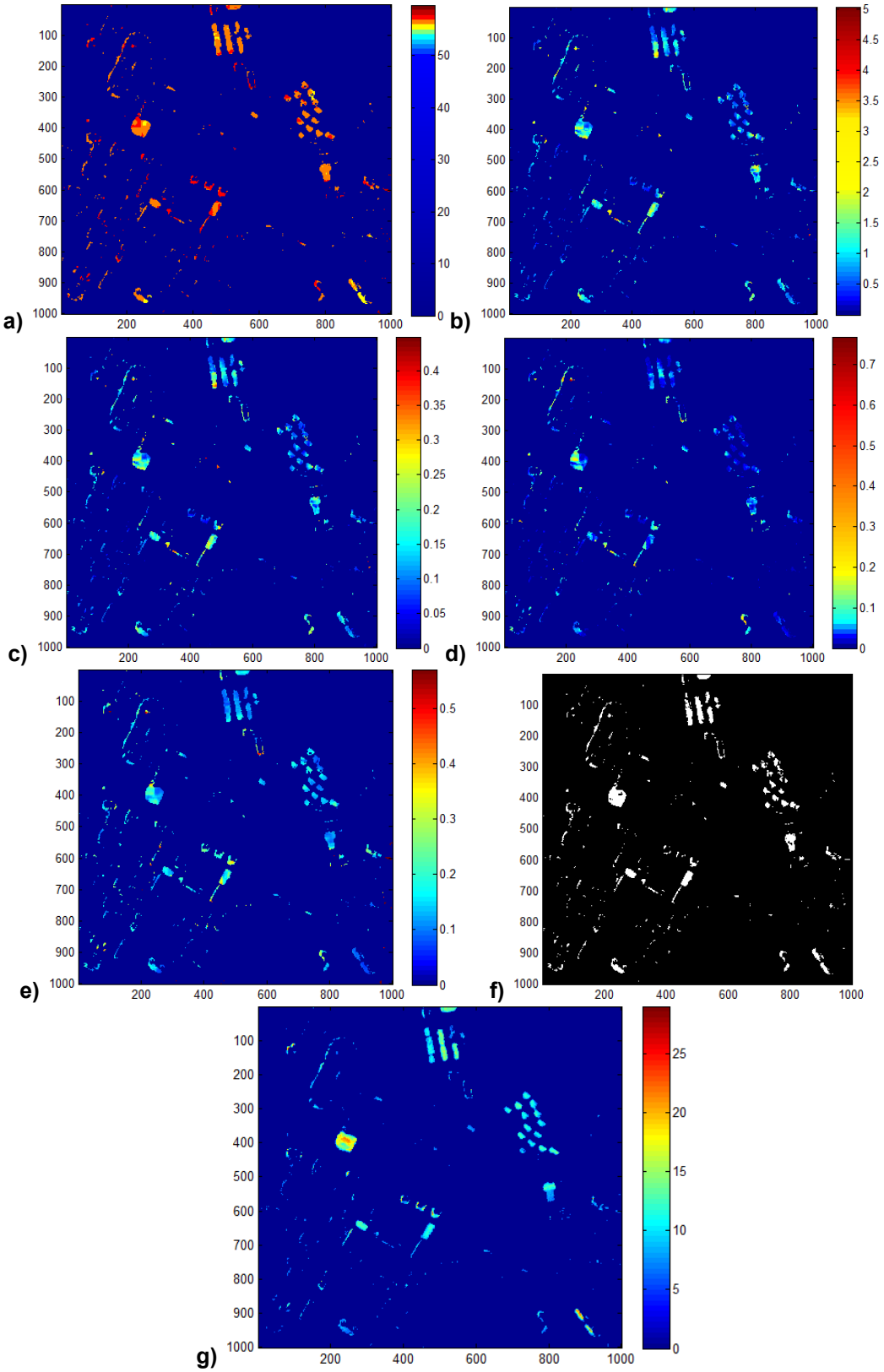

Figure 26: East Asia Data Set with seed from nonzero pixels of processed DSM difference- a) Mutual Information, b) Kullback Leibler Divergence, c) Jenson Shannon Divergence, d) Chi-Square Divergence, e) Cluster Reward Algorithm Index, f) Processed Unrefined Binary Change Map, g) Processed DSM difference

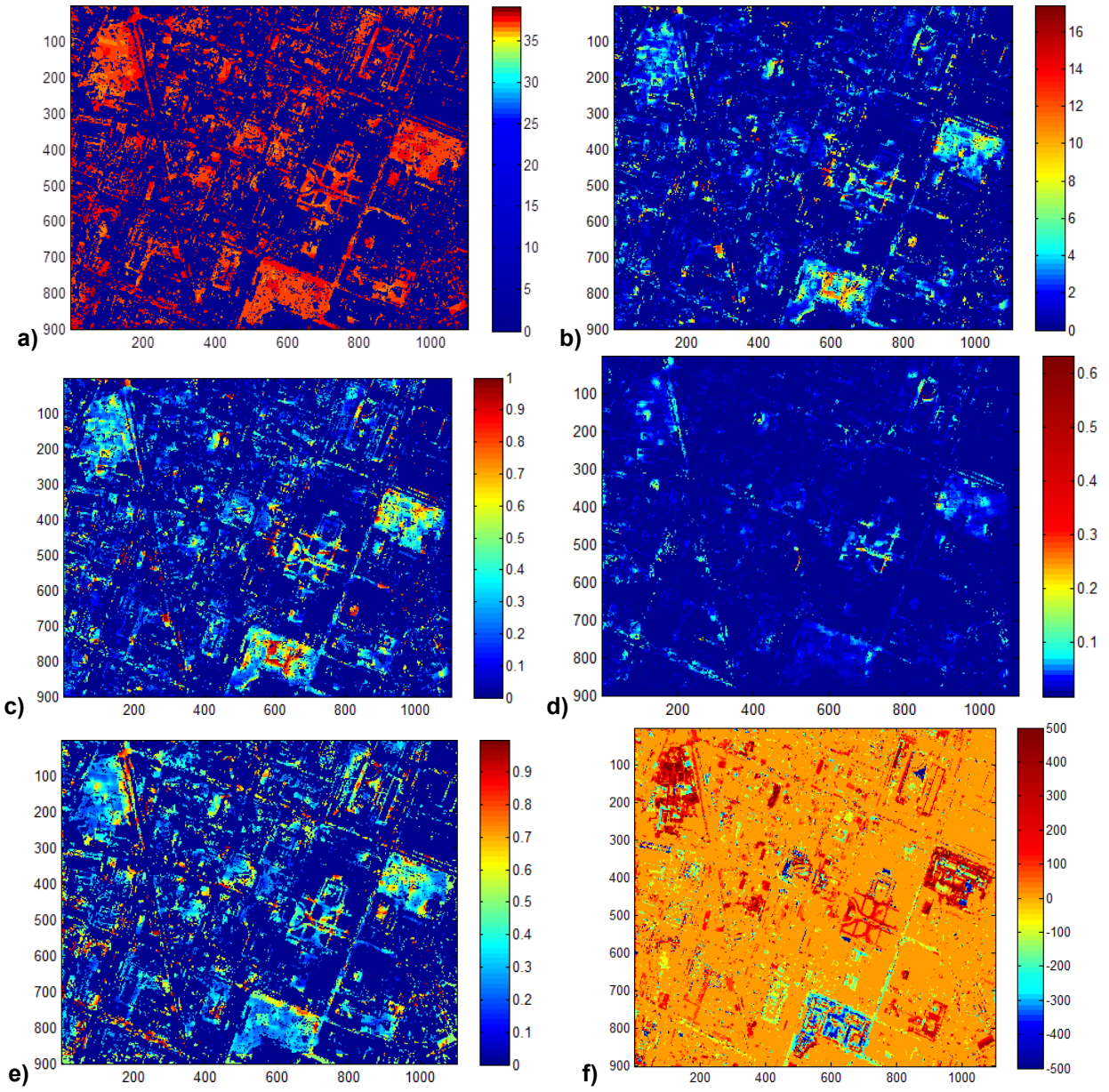

Figure 27: Munich Data Set with seed from nonzero pixels of processed Image difference- a) Mutual Information, b) Kullback Leibler Divergence, c) Jenson Shannon Divergence, d) Chi-Square Divergence, e) Cluster Reward Algorithm Index, f) Processed Image Difference

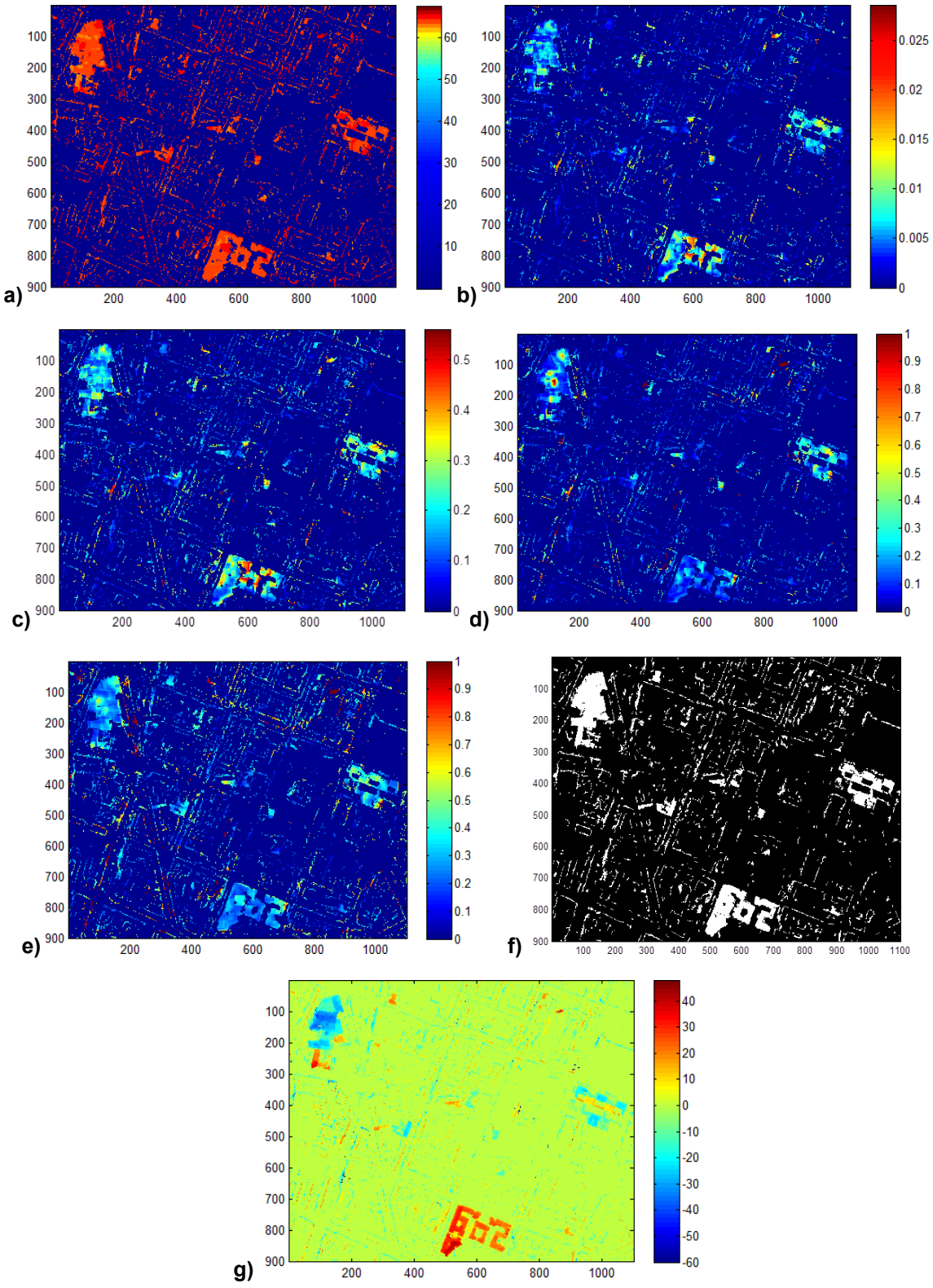

Figure 28: Munich Data Set with seed from nonzero pixels of processed DSM difference- a) Mutual Information, b) Kullback Leibler Divergence, c) Jenson Shannon Divergence, d) Chi-Square Divergence, e) Cluster Reward Algorithm Index, f) Processed unrefined binary change map, g) Processed DSM Difference

The next step in secondary change detection is to estimate the tradeoff parameter. From equation 23, there are two possible unknowns i.e. mixed information I_α and the tradeoff parameter α**.** With the four window sizes, four equations can be formed from equation 23 and thus an over determined system. This over determined system of solutions is to be solved using weighted least squares, where the weights are selected based upon the variances. This provides us with both mixed information and the tradeoff parameter. However, the obtained tradeoff parameter is discarded and recalculated using another weighted least squares. In this case the over determined system of equations has each element in the parameter set replacing the mutual information ***I*** and only one unknown i.e. the tradeoff parameter**.** Again the weights are calculated based upon the variances. Since all the information similarity measures indicate the similarity between two variables, it is valid to commence with such an action. Also it is to be noted that to match the magnitude values within the individual elements of the parameter set, normalization is crucial. For example the KLD usually has high magnitude for changed pixels while the chi-square divergence is mostly restricted near zero for the same changed pixel. From the obtained tradeoff parameter, the change map can be developed from equation 25. Even though most prominent changes appear in the change map, there are often small spots of false building changes or single pixels which correspond to noise especially when interested in buildings, they can be easily discarded. In order to remove them morphological operations are performed. Firstly all the objects are labeled and then the number pixels and the connectivity between then are checked. After selecting a max object size $S_{\max}$ for objects removal, the various objects in the change map are checked and if they fall within the selected maximum object size, and then they are eliminated. Thus the blobs in the change map retain their original shapes unlike with morphological opening operation (see Appendix B).

Figure 29 a) shows the crude change map after the secondary change detection for the East Asia data set. As mentioned already this crude change map contains noise. This is further visible in Figure 30 a) which shows the change map after secondary change detection for the Munich Data set. Figure 29 b) and c) shows the refined change map with $S_{\max}$ = 300 and $S_{\max}$ = 700 the reference data respectively. Figure 30 b) contains almost all the buildings as seen in the reference data and should be good for the object based analysis however for the pixels based analysis it may suffer severely. In figure 30 c), by increasing the parameter $S_{\max}$ = 1000 almost all the noisy areas are removed; however some of the real changed buildings are missed. Again this result shall prove better for pixel based analysis than object based analysis. Hence depending upon the utility and need the parameter $S_{\max}$ can be varied.

In figure 30 b), c) and d) the red colored buildings indicate the positive changes in buildings while the blue colored ones indicate the negative changes. It can be perceived that the nature of changes is not classified correctly to a certain extent even in the refined change map. This is true specifically for the building shown in the upper left corner see figure 31 a) and b).

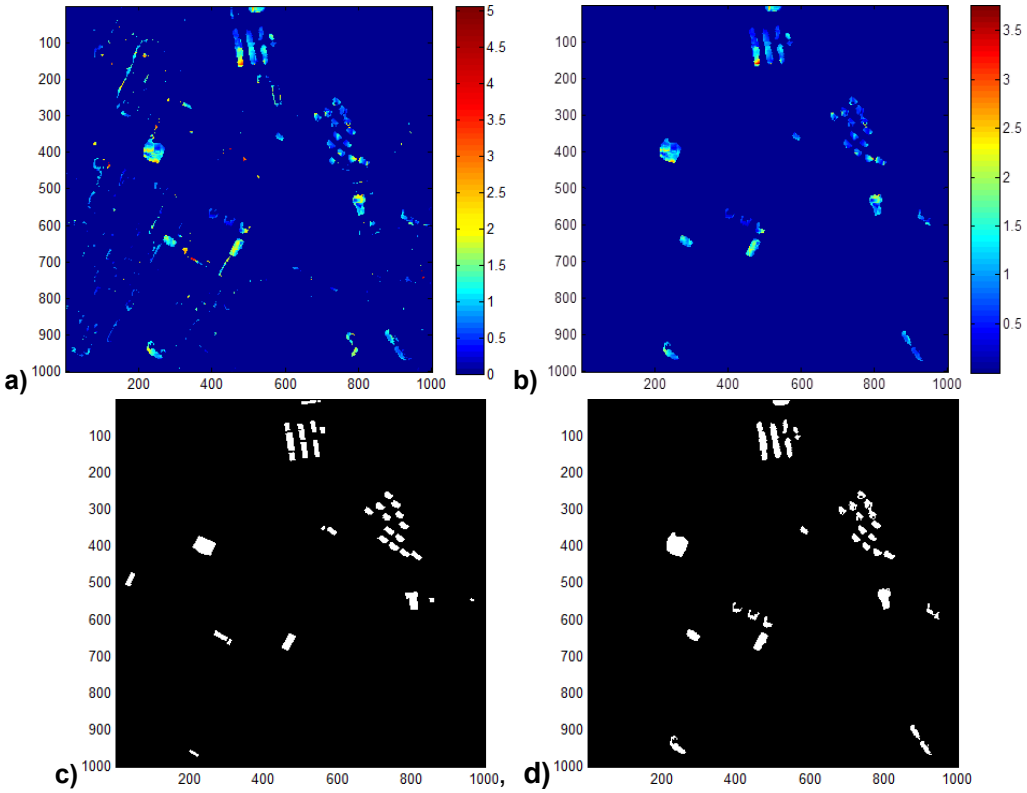

Figure 29: East Asia Data Set –a) Change Map from Secondary Detection, b) Change Map after refinement, c) Reference data, d) Binary Change Mask

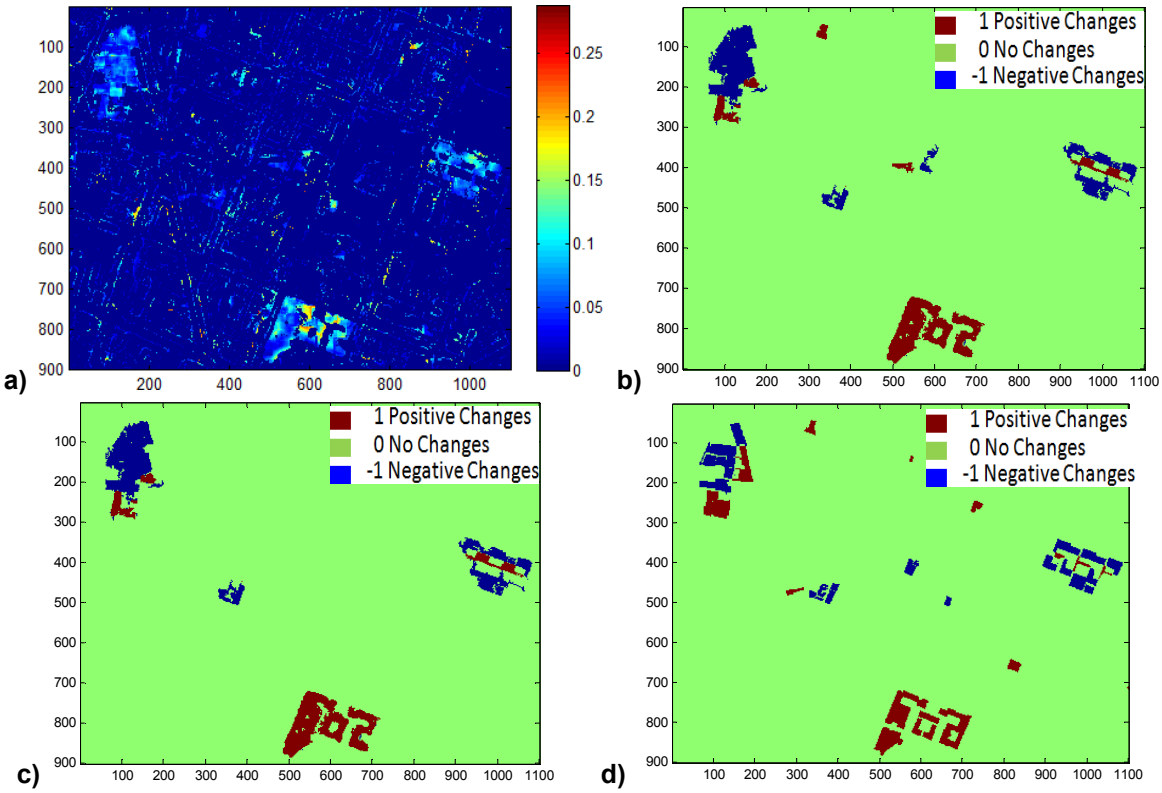

Figure 30: Munich Data Set –a) Change Map from Secondary Detection, b) Change Map after refinement with S_{max} = 300, c) Change Map after refinement with S_{max} = 1000, d) Reference data

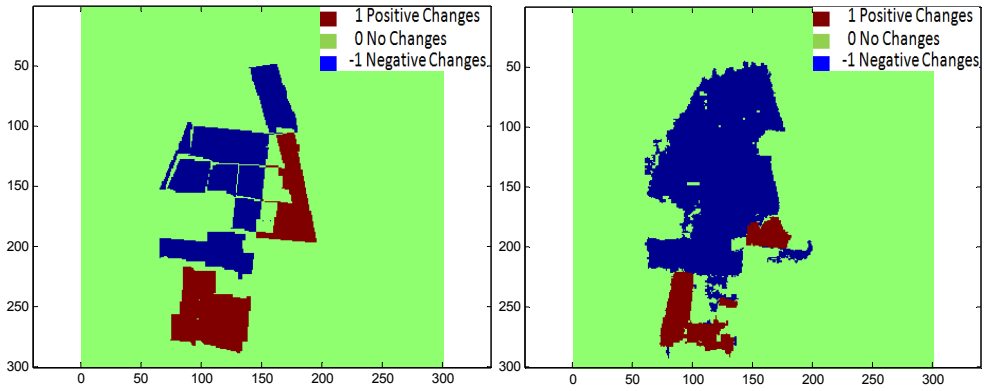

Figure 31: Munich Data Set-Left: A Building from reference data, Right: Corresponding appearance in change map

In figure 32 and 33 the buildings that are missed in the change map and those falsely detected changed buildings which are detected in the change map are shown. In figure 32, the overlay of reference data and the change map shows that 5 buildings are missed while 7 falsely detected changed buildings are detected. Similarly in figure 33 also 5 buildings are missed and 2 falsely detected changed buildings are detected. It is to be noted that during the object based assessment the group of buildings in proximity are considered one for simplicity in analysis.

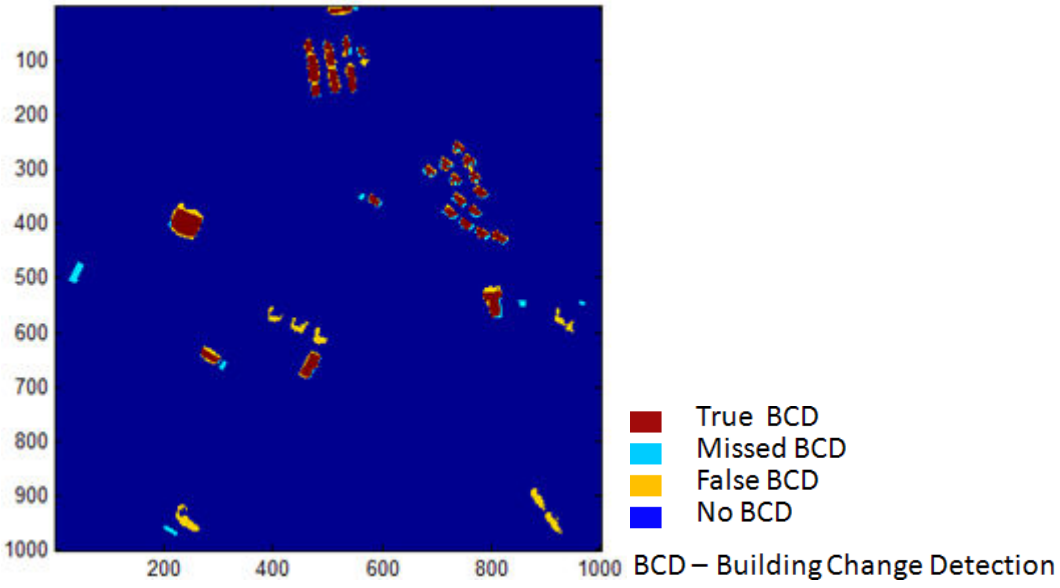

Figure 32: East Asia Data Set-Left: Unreal changed buildings detected, Right: Changed buildings missed.

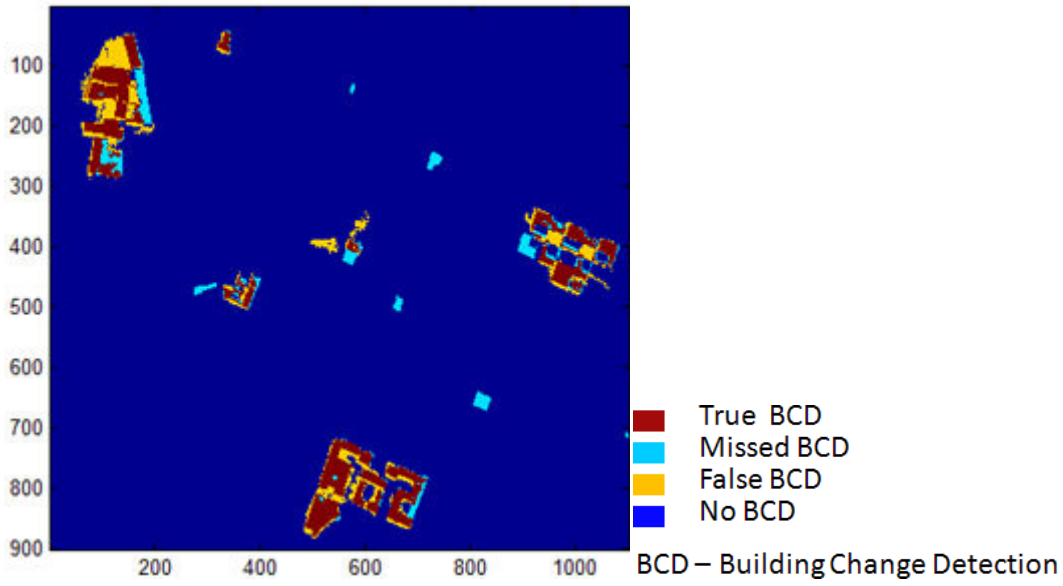

Figure 33: Munich Data Set-Left: Unreal changed buildings detected, Right: Changed buildings missed.

5. RESULT ASSESSMENT AND DISCUSSION

In this section the assessment of the results presented in previous chapter is carried out and discussed. As mentioned in section 2.4.6, for the assessment both pixel based and object based analysis is carried out between the developed change map and reference data. In literature (Jahari et al. 2008), information similarity measures are thresholded to identify the real changes. The information similarity measures are compared individually after thresholding with Otsu's Method with the developed change map and that estimated with image difference without using shadow and vegetation elimination. Also, it is to be noted that the compared information similarity measures were not processed for errors due to shadows and vegetation. Another comparison is provided with varying values of the parameter $S_{\max}$.

5.1. Results from the East Asia Data set

For the East Asia data set, results of pixel based assessment are shown in Table 6 and Table 7. Table 6 shows the confusion matrices for the refined change map and the information similarity measures used in the mentioned approach in Chapter 2. Table 7 shows the quality assessment based upon Table 6. The best results are obtained for the refined change map with $S_{\max}$ parameter set to 280. For the information similarity features in Table 6 and 7, various values for the $S_{\max}$ parameter were tested and the best approximate was selected. The information similarity measures were thresholded by the Otsu's method. In this case a correctness of 81.32 percent is achieved with a completeness of 64.61 percent and kappa accuracy of 0.71. This proves to be fairly acceptable. The overall accuracy is seen to be over 98 percent in all cases. However it is not a reliable measure for assessment as mentioned already. The overall accuracy also takes into account the similar no change pixels in both the reference data and the change map while the number of these pixels is presumably very high in most cases.

Table 6: Confusion Matrix for East Asia Data Set

Result	Confusion Matrix		
Change Map \Reference Data		Change	No Change
Refined Change Map	Change	12591	2893
	No Change	6896	980513
Change Map Without DSM	Change	6002	9482
	No Change	320990	673008
Mutual Information	Change	6002	9482
	No Change	320991	673007
Kullback Leibler Divergence	Change	3393	12091
	No Change	153369	843238
Jenson Shannon Divergence	Change	4357	11127
	No Change	228703	766940
Chi-Square Divergence	Change	3317	12167
	No Change	4576	990214
Cluster Reward Algorithm	Change	6002	9482
	No Change	320983	673015

Table 7: Pixel Based Quality Assessment for East Asia Data Set according to Table 6

SN	Result	BF	MF	COMP	CORR	QP	OA	KA
1	Refined Change Map	0.5476	0.2297	64.6123	81.3162	56.2600	99.7095	0.7151
2	Change Map Without DSM	53.4805	1.5798	1.8355	38.7625	1.7837	98.6227	0.0257
3	Mutual Information	53.4806	1.5798	1.8355	38.7625	1.7837	98.6227	0.0205
4	Kullback Leibler Divergence	45.2015	3.5635	2.1644	21.9129	2.0094	98.5919	0.0256
5	Jenson Shannon Divergence	52.4909	2.5538	1.8694	28.1387	1.7842	98.5778	0.0207
6	Chi-Square Divergence	53.0994	3.6680	1.8484	21.4221	1.7310	98.5446	0.0198
7	Cluster Reward Algorithm	53.4793	1.5798	1.8355	38.7625	1.7838	98.6228	0.0205

In Table 7, the following abbreviations are used: -

BF = Branching Factor.
MF = Miss Factor.
COMP = Completeness.
CORR = Correctness.
QP = Quality Percentage.
KA = Kappa Accuracy.

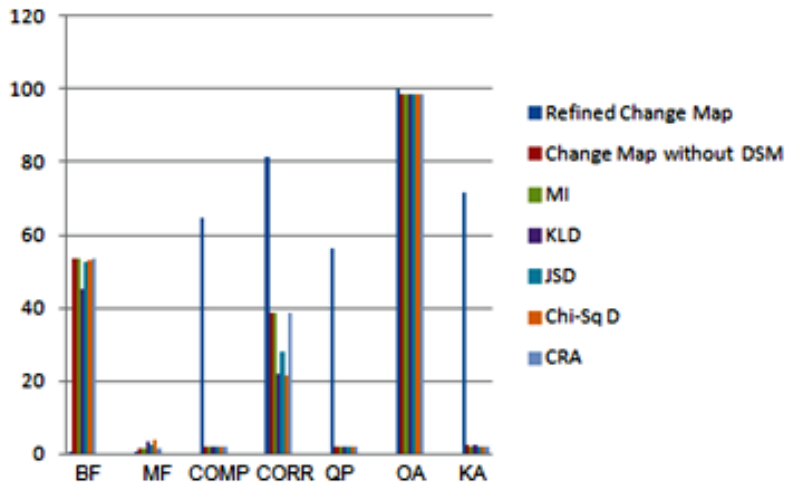

Figure 34: Comparison of Change map with other similarity features based on table 6

Figure 34 shows the comparison of the information similarity measures with the developed approach using the processed DSM difference and image difference as seed. The information similarity measures alone prove inefficient alone. As explained in chapter 4 most pixels differ appreciably in gray values in the early and late image due to the presence of snow in the late image causing poor agreement. Thus evident is the high branching factor and extremely values for other assessment parameters in figure 34. However with incorporation of the height information from DSMs it is seen that accuracy increases drastically.

Table 8: Change Map Refinement with varying values of S_{max}

Refined Change Map			
S_{max}	**Change Map \Reference Data**	**Change**	**No Change**
S_{max} = 0	**Change**	12592	2892
	No Change	17585	969823
S_{max} = 50	**Change**	12591	2893
	No Change	13869	973540
S_{max} = 100	**Change**	12591	2893
	No Change	11913	975496
S_{max} = 150	**Change**	12591	2893
	No Change	10469	976940
S_{max} = 200	**Change**	12591	2893
	No Change	9234	978175
S_{max} = 250	**Change**	12591	2893
	No Change	7444	979965
S_{max} = 300	**Change**	12591	2893
	No Change	6571	981388
S_{max} = 350	**Change**	12591	2893
	No Change	6129	983340

Table 9: Pixel Based Quality Assessment for East Asia Data Set according to Table 8

S_{max}	BF	MF	COMP	CORR	QP	OA	KA
S_{max} = 0	1.3965	0.2296	41.7271	81.3226	38.0779	99.7064	0.5421
S_{max} = 50	1.1015	0.2297	47.5850	81.3161	42.8951	99.7074	0.5924
S_{max} = 100	0.9461	0.2297	51.3834	81.3161	45.9575	99.7080	0.6225
S_{max} = 150	0.8314	0.2297	54.6010	81.3161	48.5146	99.7084	0.6467
S_{max} = 200	0.7333	0.2297	57.6907	81.3161	50.9385	99.7088	0.6689
S_{max} = 250	0.5912	0.2297	62.8450	81.3161	54.9153	99.7093	0.7037
S_{max} = 300	0.5457	0.2859	64.6948	77.7641	54.5953	99.6546	0.7012
S_{max} = 350	0.5819	0.4703	63.2112	68.0121	48.7253	99.5041	0.6496

S_{max} parameter has a similar effect to thresholding. Thus various values of S_{max} parameter were tried for the refinement and listed in Table 8 with the achieved confusion matrices. Table 9 shows the pixel based quality assessment for these various values S_{max}. Figure 35 and 36 shows the bar plot and performance curves for pixel based accuracy assessment with respect to the various values of $S_{max.}$

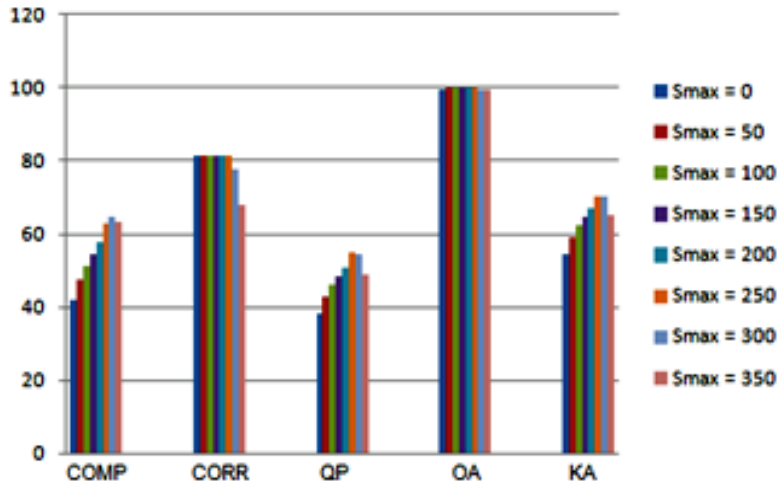

Figure 35: Pixel Based Accuracy Assessment with respect to S_{max}

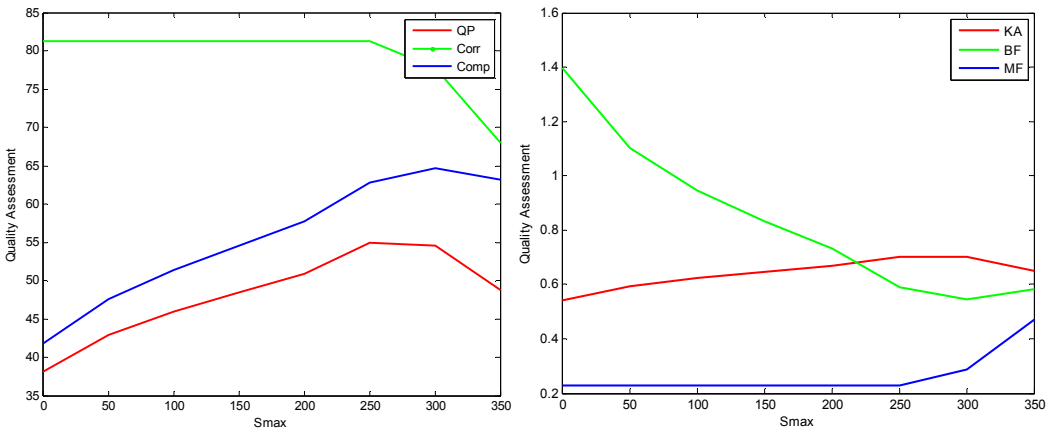

Figure 36: Performance curves for table 9.

Table 10 shows the details on the number of buildings that were detected, missed and falsely detected for the East Asia data set. According to table 10, there are 31 changed buildings at hand in the scene out of which 27 were correctly detected in the developed change map. However 7 other buildings were detected which are not associated to any real changes and 5 changed buildings were missed.

Table 10: Object Based Assessment for East Asia Data Set

BUILDING	No.
Total Buildings in Reference Data (Nr)	31
Total Buildings in Change Map (Nc)	33
True Changed Buildings in Change Map (Ntc)	27
Missing Changed Buildings (Nm)	5
Unreal Changed Buildings (Nuc)	7

Based on Table 10 the confusion matrix was implemented. For determining the true negative an approximate visual counting of all the buildings in the scene was carried out. In the East Asia data set the approximate number of buildings ***N,*** was found to be 190. And the true negative was estimated by reducing the false and true changed buildings from ***N.*** Table 12 shows the object based quality assessment for the East Asia data set based on the confusion matrix derived in table 11. An overall accuracy of 93.75% is achieved with a correctness of over 79% and a completeness of over 84%.

Table 11: Confusion Matrix for Object Based Assessment for East Asia Data Set

Change Map \Reference Data	Change	No Change
Change	27	7
No Change	5	153

Table 12: Object Based Quality Assessment according to Table 11

Result	BF	MF	COMP	CORR	QP	OA
Refined Change Map	0.2592	0.1851	84.3750	79.4117	69.2307	93.7500

5.2 Results from Munich Data set

For the Munich data set, results of pixel based assessment are shown in Table 13 and Table 14. Table 13 shows the confusion matrices for the refined change map and the information similarity measures used in the mentioned approach in Chapter 2. Table 14 shows the quality assessment based upon Table 13.

Table 13: Confusion Matrix for Munich Data Set

Result	Confusion Matrix		
Change Map \Reference Data		**Change**	**No Change**
Refined Change Map	**Change**	28903	9424
	No Change	16667	944430
Change Map Without DSM	**Change**	31231	8149
	No Change	182934	775835
Mutual Information	**Change**	31415	6912
	No Change	216151	742434
Kullback Leibler Divergence	**Change**	11288	27039
	No Change	118727	859985
Jenson Shannon Divergence	**Change**	27049	11278
	No Change	143523	819428
Chi-Square Divergence	**Change**	11905	26422
	No Change	70700	907395
Cluster Reward Algorithm	**Change**	31405	6922
	No Change	215249	743346

Table 14: Pixel Based Quality Assessment according to Table 13

SN	Result	BF	MF	COMP	CORR	QP	OA	KA
1	**Refined Change Map**	0.5766	0.3260	63.4254	75.4115	52.5566	99.0410	0.6823
2	**Change Map Without DSM**	5.8574	0.2609	14.5826	79.3067	14.0481	99.0003	0.2484
3	**Mutual Information**	6.8805	0.2200	12.6895	81.9657	12.3448	99.1147	0.1926
4	**Kullback Leibler Divergence**	10.517	2.3953	8.68207	29.4518	7.18733	96.9900	0.1074
5	**Jenson Shannon Divergence**	5.3060	0.4169	15.8578	70.5742	14.8743	98.6851	0.2476
6	**Chi-Square Divergence**	5.9386	2.2194	14.4119	31.0616	10.9193	97.2061	0.1750
7	**Cluster Reward Algorithm**	6.8397	0.2204	12.7324	81.9396	12.3848	99.1144	0.1933

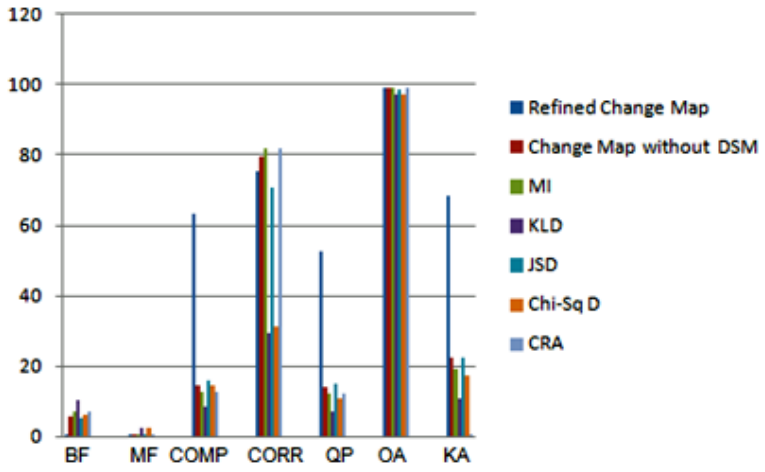

Figure 37: Comparison of Change map with other similarity features based on table 6: a) Correctness, b) Completeness, c) Kappa Accuracy

The best results are obtained for the refined change map with $S_{\max}$ parameter set to 700. For the information similarity features in Table 13 and 14, various values for the $S_{\max}$ parameter were tried and the nearly best approximate was selected. In this case a correctness of 75.41 percent is achieved with a completeness of 63.42 percent and kappa accuracy of 0.682. Again the tradeoff between completeness and correctness was seen. The information similarity measures were thresholded by the Otsu's method. The poor results could be attributed to the resolution difference in the two images. Also it must be noted that holes in the joint probability appears as noise in information similarity measure incorporating the joint probability. Since the joint probability in this study was developed from histogram many holes were observed.

Table 15: Change Map Refinement with varying values of $S_{\max}$

Refined Change Map			
$S_{\max}$	**Change Map \Reference Data**	**Change**	**No Change**
$S_{\max}$ = 0	**Change**	30248	8079
	No Change	95273	864479
$S_{\max}$ = 50	**Change**	29992	8335
	No Change	41189	918819
$S_{\max}$ = 100	**Change**	29838	8489
	No Change	28476	931686
$S_{\max}$ = 150	**Change**	29793	8534
	No Change	23968	936239
$S_{\max}$ = 200	**Change**	29175	9152
	No Change	19959	940866
$S_{\max}$ = 250	**Change**	28903	9424
	No Change	16667	944430
$S_{\max}$ = 300	**Change**	28405	9922
	No Change	15722	945873
$S_{\max}$ = 350	**Change**	28085	10242
	No Change	30248	8079

Table 16: Pixel Based Quality Assessment for East Asia Data Set according to Table 15

S_{max}	BF	MF	COMP	CORR	QP	OA	KA
S_{max} = 0	3.1497	0.2670	24.0979	78.9208	22.6407	99.1051	0.35034
S_{max} = 100	1.3733	0.2779	42.1348	78.2529	37.7181	99.1291	0.53622
S_{max} = 200	0.9543	0.2845	51.1678	77.8511	44.6656	99.1248	0.6084
S_{max} = 300	0.8044	0.2864	55.4174	77.7337	47.8256	99.1243	0.63891
S_{max} = 500	0.6841	0.3136	59.3784	76.1212	50.0549	99.0653	0.65979
S_{max} = 700	0.5766	0.3260	63.4254	75.4115	52.5566	99.0410	0.68235
S_{max} = 900	0.5534	0.3493	64.3710	74.1122	52.5541	98.9918	0.68245
S_{max} = 1000	0.5378	0.3646	65.0251	73.2773	52.5611	98.9603	0.68256

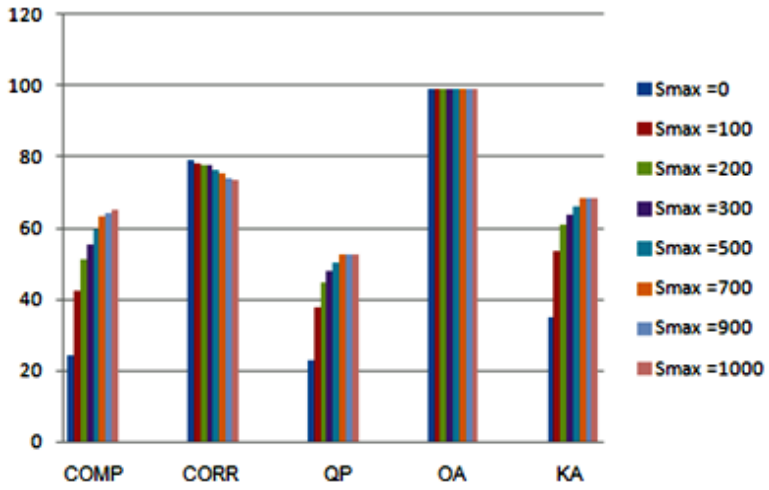

Figure 38: Pixel Based Accuracy Assessment with respect to S_{max}

In Table 15, various values of S_{max} parameter were tried for the refinement and the achieved confusion matrices are listed. Table 16 shows the pixel based quality assessment for these various values S_{max}. It is observed that the correctness reduces linearly while the completeness increases linearly with increase in the S_{max} parameter. A similar trend is seen with the branching factor and the miss factor.

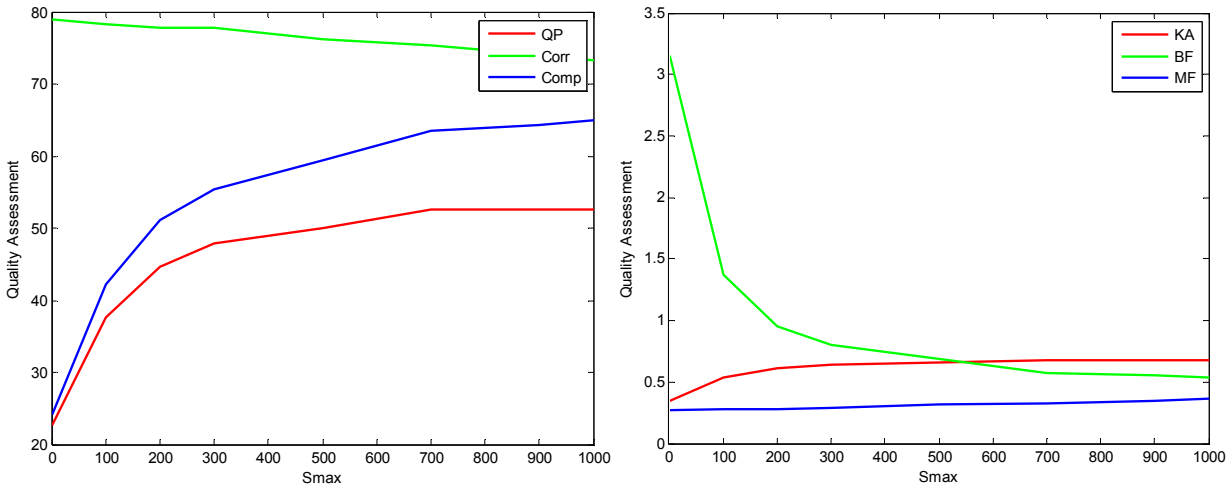

Figure 39: Performance curves for table 16

Table 17: Object based assessment for East Asia Dataset

BUILDING	**No.**
Total Buildings in Reference Data (Nr)	11
Total Buildings in Change Map (Nc)	8
True Changed Buildings in Change Map (Ntc)	6
Missing Changed Buildings (Nm)	5
Unreal Changed Buildings (Nuc)	2

Table 17 shows the number of changed buildings detected, missed or falsely detected for the Munich data set. In Table 17, there are 11 changed buildings at hand in the scene out of which 6 were correctly detected in the developed change map. However 5 buildings were missed, of which some are of comparatively very small size. Also 2 falsely detected changed buildings were detected. It is to be noted that for simplicity some of the buildings in very close proximity were considered as one for the assessment. There are three such clusters in the Munich data set as seen in figure 36. This was done to simplify the assessment, since it is a very complicated procedure to actually separated individual buildings from these clusters in the change map even with visual counting. Since even visually it was difficult to identify the boundaries of many buildings which appeared in clusters in the satellite images.

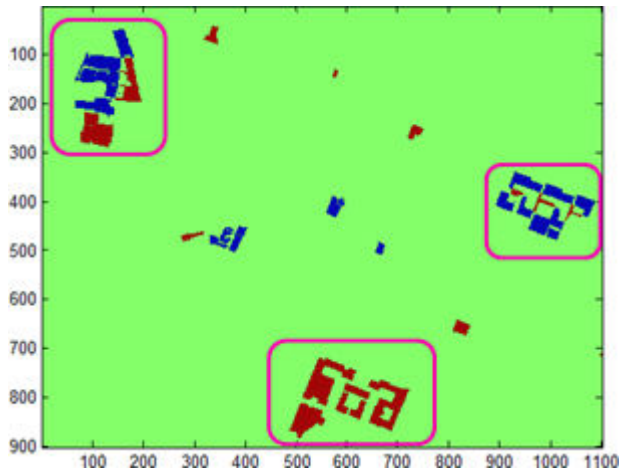

Figure 40: Clusters of buildings that were considered as single buildings for the Object Based Assessment

Table 18: Confusion Matrix for Object Based Assessment

Change Map \Reference Data	Change	No Change
Change	6	2
No Change	5	202

Table 19: Quality Assessment from Table 18

SN	BF	MF	COMP	CORR	QP	OA
Refined Change Map	0.3333	0.8333	54.5454	75.0000	46.1538	86.3070

Based on Table 17 the confusion matrix was implemented in table 18. For determining the true negative an approximate visual counting of all the buildings in the scene was carried out. In the Munich data set the approximate number of buildings ***N,*** was found to be 210. And the true negative was estimated by reducing the false and true changed buildings from ***N.*** Table 19 shows the object based quality assessment for the East Asia data set based on the confusion matrix derived in table 18. An overall accuracy of 86.307% is achieved with a correctness of over 75% and a completeness of nearly 55%.

6. CONCLUSION

The objective of this work was to develop a method for change detection in remote sensing images from high resolution satellites with incorporation of height information from the DSMs. Another objective of this work was to test the suitability of various information measures for change detection. It is well known in literature that classical image differencing is not sufficient for change detection in urban areas (Bruzzone & Prieto 2000). In simple image differencing, when the gray values of two images are similar they are regarded as no change areas. However in real situations this may not be the case. Thus a means to enhance the change detection from classical image differencing is of need. Information similarity measures provide us with a metric to adapt the decision regarding the hypothesis for changed pixels. They not only consider the gray values of concerned pixels but also their surroundings to develop a decision, when used in a sliding window algorithm. The experiments in the East Asia data showed that such measures regarded areas covered with snow as changes which were easily eliminated with the help of DSM or even with simple thresholding. The major advantage of using these techniques is that simply the gray level information from the images for decision regarding change detection is required along with the DSMs.

In this study the various information similarity measures were tested to produce a change map and compared without shadow and vegetation removal against the developed change map. In case of the East Asia data set, it was seen that none of the information similarity measures could provide any satisfactory results by them. For the Munich data set also, the information similarity measures used in this study were barely able distinguish between real and false building changes to some extent. The test data for this study had certain flaws, such as the snow mentioned earlier in East Asia data set and the appearance of skeletal structures due to the resolution difference in the Munich data set. Some of these structures are associated to the changes in vegetation in the Munich data set (not eliminated for comparison of individual information similarity measures with the developed change map). In such cases the information similarity measures regard these erroneous regions as feasible changes. Thresholding in such a case is always a tradeoff between missed detections and false alarms. However, morphological operations, as those used in this study can significantly reduce errors and noise appearing as small regions in the change map. The removal of smaller regions is effective, since the desired changed regions appearing as blobs corresponding to buildings are unaffected. The dependency of the developed approach for 2D building change detection upon these measures renders the accuracy of building change detection restricted. Also, the estimation of the information similarity measures is highly dependent upon the probability estimation. Although histogram is a simple means of extracting the probability density for a distribution, it fails to model the distribution to a satisfactory precision thus increasing the ambiguity associated to the classification of changes. However, when height information from the DSM is incorporated in the methodology, significant improvement is observed. Hence the information from the DSMs proved extremely crucial in building change detection. The experimental results show that although some smaller buildings are omitted in detection as in case of the Munich data most of the other buildings are normally detected to a sufficient degree so as to reconstruct their shape.

And usually none or very few falsely detected changed buildings were seen with change detection amongst all the data sets.

Also it has to be mentioned that the changes in the Munich data set is complicated even to be analyzed by visual interpretation. The manual visual interpretation for generating the reference data is solely an attribute of the user. The overall accuracy was relatively very high due to a large number of true negatives in change detection, which however is unreliable as a means to evaluate an algorithm. A better means of evaluation was thus considering the correctness and completeness together or assessing the quality percentage. However, the accuracy of a change detection algorithm always occurs as a tradeoff between correctness and completeness, increasing one cause reduction in the other. Although pixel based analysis is the standard method for assessing the effectuality of any change detection algorithm, very often it deludes significant facts. Hence in such cases the object based analysis is significant. For this study the object based analysis of results proved evidently sufficient.

The accuracy of an algorithm largely rests on the accuracy of the reference data. Reference data is often used in multiple ways. Usually reference data is used to evaluate different methodologies, but the same can be used to supervise algorithms. In supervised methods training data provides a means to separate changed regions from unchanged ones. In this work training data is used to estimate the optimum window sizes for the various information measures. Similar but little inferior results could well be achieved with assuming generalized window sizes for the neighborhood processing. However analysis with training data was required within this work for selection of window sizes. The training regions selected merely fall within the size of 50 pixels. These pixels can well be selected from the thresholded DSMs, thus evading the requirement of reference data for training data in this case. After analysis of these training areas for all the data sets, specific range of window sizes were specified in section 4.2.1, this information can be used further for any other data sets used.

Overall it can be said that the mentioned approach can sufficiently distinguish between changed and unchanged buildings. The concerned approach poses a powerful technique that utilizes simply the information from DSMs and pixel gray values from early and late images.

7. FUTURE WORK

In this study various high and low level information similarity measures were used such as mutual information and chi-square divergence respectively. In this approach, firstly the histograms were used to obtain the probability density for the sliding window algorithm. However, the obtained joint probability seemed to be sparse. It is suggested to use other methods for probability density estimation such as the semi-parametric methods used by Bruzzone & Prieto (2002) or that suggested by Rajwade et al. (2009). Also another area of testing the robustness of this approach would be experimentation with other data sets. The approach could also be tested with SAR images. Since information similarity measures are often used with SAR data for change detection, theoretically the applicability of this method to SAR data should be significantly effective. It would be of interest to analyze this approach with different window shapes for the sliding window algorithm and incorporation of homogeneity as a decision parameter.

REFERENCES

Alberga V (2009) Similarity Measures of Remotely Sensed Multi-Sensor Images for Change Detection Applications. Remote Sensing 1 (3): 122-143.

Benedek, C, Descombes X, Zerubia J (2009) Building extraction and change detection in multitemporal remotely sensed images with multiple birth and death dynamics. IEEE Workshop on Applications of Computer Vision, Nice France: 1-6.

Bruzzone L & Prieto D (2000) Automatic analysis of the difference image for unsupervised change detection. IEEE Transactions on Geoscience and Remote Sensing 38 (3): 1171-1182.

Chaabouni-Chouayakh H, d'Angelo P, Krauß T, Reinartz P (2011) Automatic urban area monitoring using digital surface models and shape features. Joint Urban Remote Sensing Event. IEEE: 85-88.

Choi E & Lee C (2003) Feature extraction based on the Bhattacharyya distance. Pattern Recognition 36 (8): 1703-1709.

Congalton R (1991) A review of assessing the accuracy of classifications of remotely sensed data. Remote Sensing of Environment 37 (1): 35-46.

Cui S, Datcu M, Gueguen L (2011) Information theoretical similarity measure for change detection. Joint Urban Remote Sensing Event. Munich, Germany: 69-72.

d'Angelo P (2010) Image Matching and Outlier Removal For large Scale DSM Generation. In: Convergence in Geomatics. CGC & ISPRS. ISPRS Symposium Commission I, Calgary, Canada: 15-18.

Elvidge C.D, Yan D, Ridgeway D.W, and Lunetta R.S (1995) Relative radiometric normalization of Landsat Multispectral Scanner (MSS) data using an automatic scattergram controlled regression. Photogrammetric Engineering & Remote Sensing, ASPRS 61(10): 1255-1260.

Erten E, Reigber A, Hellwich O (2010) Aspects of multivariate statistical theory with the application to change detection. IEEE, International Geoscience and Remote Sensing Symposium. Honolulu, HI: 1960-1963.

Goldberger J, Gordon S, Greenspan H (2003) An efficient image similarity measure based on approximations of KL-divergence between two gaussian mixtures. Proceedings Ninth IEEE International Conference on Computer Vision (1): 487-493.

Grosse I, Bernaola-Galván P, Carpena P, Román-Roldán R, Oliver J, Stanley H (2002) Analysis of symbolic sequences using the Jensen-Shannon divergence. Physical Review E, American Physics Society 65 (4), 041905-041931.

Gueguen L, Cui S, Schwarz G, Datcu M (2010) Multitemporal analysis of multisensor data: Information theoretical approaches. IEEE International Geoscience and Remote Sensing Symposium. Honolulu, HI: 2559-2562.

Gueguen L, Soille P, Pesaresi M (2011) Change Detection Based on Information Measure. IEEE Transactions on Geoscience and Remote Sensing PP(99), 1-13.

Hirschmüller H (2008) Stereo Processing by Semiglobal Matching and Mutual Information. IEEE Transactions on Pattern Analysis and Machine Intelligence 30 (2), 328-341.

Inglada J & Giros A (2004) On the possibility of automatic multisensor image registration. IEEE Transactions on Geoscience and Remote Sensing 42 (10), 2104-2120.

Inglada J (2009) Change detection on SAR images by using a parametric estimation of the Kullback-Leibler divergence. Proceedings of International Geoscience and Remote Sensing Symposium. Naples, Italy: 4104-4106.

Jahari M, Khairunniza-Bejo S, Shariff A.R.M, Shafri H.Z.M, Ibrahim H (2008) Change detection using a local similarity measure. IEEE Conference on Innovative Technologies in Intelligent Systems and Industrial Applications. Cyberjaya, Malaysia: 39-43.

Tian J, Sun J, Tang Y (2009) Tricolor Attenuation Model for Shadow Detection. IEEE Transactions on Image Processing 18 (10), 2355-2363.

Kim J, Kolmogorov V, Zabih R (2003). Visual correspondence using energy minimization and mutual information. Proceedings of Ninth IEEE International Conference on Computer Vision. Nice, France vol.2, 1033-1040.

Krauß T, Reinartz P, Stilla U (2007) Extracting Orthogonal Building Objects in Urban Areas from High Resolution Stereo Satellite Image Pairs. International Archives of Photogrammetry, Remote Sensing and Spatial Information Sciences, 36, Part 3/W49B: 77-83.

Lafaix J & Bosser L (2009) A new change detection algorithm for SAR images., Radar Conference - Surveillance for a Safer World, RADAR International. Bordeaux, France: 1-8

Lin Z, Hideki S, Kikuo T, Zhen L, Gong P (2009) Building change detection using aerial images and existing 3D data. Joint Urban Remote Sensing Event. Shanghai, China: 1-5.

Lu D, Mausel P, Batistella M, Moran E (2005) Land-cover binary change detection methods for use in the moist tropical region of the Amazon: a comparative study. International Journal of Remote Sensing 26 (1), 101-114.

Mas J.-F (1999) Monitoring land-cover changes: A comparison of change detection techniques. International Journal of Remote Sensing 20 (1), 139-152.

Mercier G, Inglada J (2008) Change Detection with Misregistration Errors. IGARSS 2008 - 2008 IEEE International Geoscience and Remote Sensing Symposium. Boston, MA: III - 154 - III - 157.

Okhandiar R.R, Raju P.L.N and Bijker W (2008) Neighborhood correlation image analysis technique for change detection in forest landscape. In: ISPRS: Proceedings of the XXI congress: Silk road for information from imagery: the International Society for Photogrammetry and Remote Sensing, Commission VIII, WG VIII/11. Beijing, China: ISPRS, 2008. pp. 1031-1037.

Pagot E, Pesaresi M (2008) Systematic Study of the Urban Postconflict Change Classification Performance Using Spectral and Structural Features in a Support Vector Machine. IEEE Journal of Selected Topics in Applied Earth Observations and Remote Sensing 1 (2), 120-128.

Patricio M.P, Cabestaing F, Colot O, Bonnet P (2004) A similarity based adaptive neighborhood method for correlation based stereo matching. International conference on Image Processing. Villeneuve d'Ascq, France, vol. 2: 1341-1344.

Radke R, Andra S, Al-Kofahi O, Roysam B (2005) Image change detection algorithms: a systematic survey. IEEE Transactions on Image Processing 14 (3), 294-307.

Rajwade A, Banerjee A, Rangarajan A (2009) Probability Density Estimation Using Isocontours and Isosurfaces: Applications to Information-Theoretic Image Registration. IEEE Transactions on Pattern Analysis and Machine Intelligence 31 (3), 475-491.

Singh A (1989) Review Article Digital change detection techniques using remotely-sensed data. International Journal of Remote Sensing 10 (6), 989-1003.

Suri S & Reinartz P (2010) Mutual-Information-Based Registration of TerraSAR-X and Ikonos Imagery in Urban Areas. IEEE Transactions on Geoscience and Remote Sensing 48 (2), 939-949.

Tian J, Chaabouni-Chouayakh H, Reinartz P, Krauß T, d'Angelo P (2010). Automatic 3d Change Detection Based On Optical Satellite Stereo Imagery. In: International Archives Of The Photogrammetry, Remote Sensing and Spatial Information Sciences. ISPRS Technical Commision VII Symposium. Vienna, Austria 38 (7B): 586-591.

Tian J, Chaabouni-Chouayakh H, Reinartz P (2011) 3D Building Change Detection from High Resolution Spaceborne Stereo Imagery. International Workshop on Multi-Platform/Multi-Sensor Remote Sensing and Mapping. Xiamen, China: 1-7.

APPENDIX A: THRESHOLDING

1. Otsu's Method for Thresholding

Otsu's thresholding method involves using the histogram to separate pixels into foreground and background. The method involves checking all possible thresholds and measuring the spread for pixel levels on either side of the threshold. The threshold value where the sum of foreground and background spreads minimizes is selected as the initial threshold.

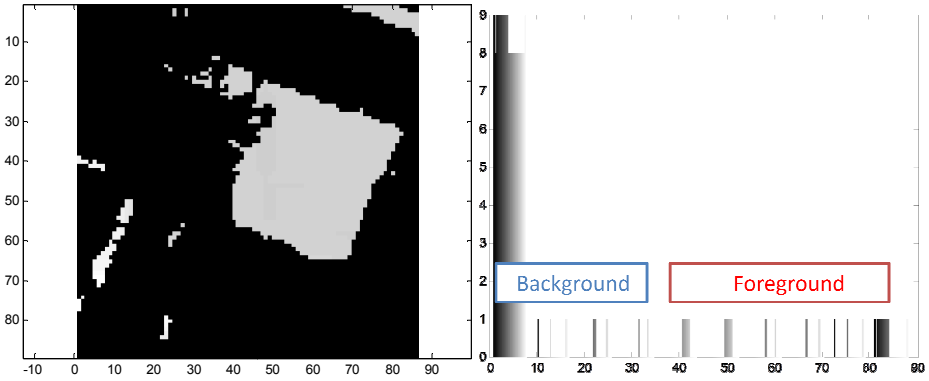

Figure 41: Example: Image and histogram sorted into foreground and background.

2. Interactively selecting the threshold

The thresholds can be selected by shifting the thresholds from the Otsu's method and simultaneously checking the thresholded binary image. This can be achieved using the thresholding tool under "thresh_tool" (Copyright (c) 2009, The MathWorks, Inc.Copyright (c) 2001, Brandon Kuczenski. All rights reserved.) available at the matlab file exchange. In order to select the thresholds individually for the negative and positive sections of an image firstly the image *Xd* is separated into two matrices with each having positive and negative values from the image *Xd* (equation 30) i.e. X_{d+} & X_{d-} respectively and then the thresholds for the image *Xd* are derived by thresholding these two matrices as shown in figure 25.

$X_{d_+} = Xd$ Initialization of the Positive mask

$X_{d-} = Xd$ Initialization of the negative mask

$X_{d_+}(X_{d_+} < 0) = 0$ Setting all values <0 as 0

$X_{d-}(X_{d-} > 0) = 0$ Setting all values >0 as 0

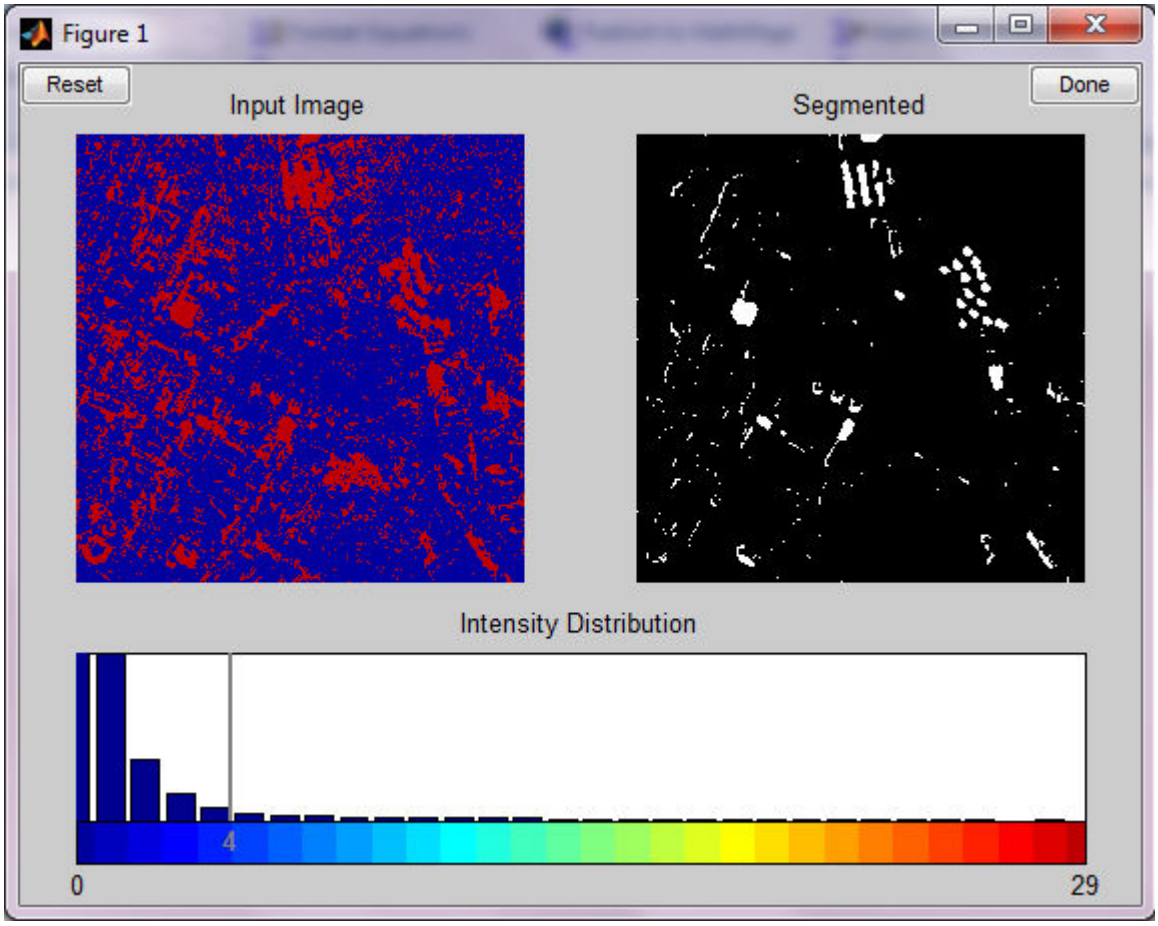

Figure 42: Thresholding X_{d+}

APPENDIX B: REMOVING SMALL REGIONS

Morphological operations are often used in change detection for removal of noise and filling holes. The commonly used methods are 'opening', 'closing', 'dilation' and 'erosion'. In the presented approach morphological area opening is used to remove smaller regions from the change map. The matlab function 'bwareaopen' is used for this purpose (http://www.mathworks.com/help/toolbox/images/ref/bwareaopen.html). Matlab is a user friendly numerical computing environment and a fourth generation programming language developed by Mathworks. Although 'bwareaopen' is referred to simply as morphological opening, this function removes smaller regions based on connectivity between pixels.

Firstly all the objects in the given image are labeled in the set L (L0, L1, L2 ……Ln). Then the total number of pixels in each object is calculated based on the immediate connectivity. The immediate connectivity 'c' is specified by the used to be either '2'or '4'. The algorithm searches for 2 or 4 connecting neighbors respectively and counts the number of pixels in an object. Furthermore a maximum object size is specified for removal by the user. Thus any objects of size greater than this maximum object size would be retained while the others would be eliminated. The entire process is followed for all the objects in the given image.

Follwing is the pseudo code for the operation of this algorithm:

Input: Image - Im (containing n objects), connectivity c='2' or '4',
Maximum region size=' $S_{\max}$'

Step1: Set Labels for each object.
Label set (L0, L1, L2 ……Ln).
Step 2: Pop label
Step 3: Check connectivity and count the number of pixels in the region (Np).

If Np > $S_{\max}$
Do nothing
else
Eliminate Region.
Step 4: Return to step 2.
If last label
end.